

Hunting for Extremely Faint Planetary Nebulae in the SDSS Spectroscopic Database

H. B. Yuan^{1*}† & X. W. Liu^{1,2}

¹ *Kauli Institute for Astronomy and Astrophysics, Peking University, Yi He Yuan Road 5, Hai Dian District, Beijing 100871, China*

² *Department of Astronomy, Peking University, Yi He Yuan Road 5, Hai Dian District, Beijing 100871, China*

Received:

ABSTRACT

Using $\sim 1,700,000$ target- and sky-fiber spectra from the Sloan Digital Sky Survey (SDSS), we have carried out a systematic search for Galactic planetary nebulae (PNe) via detections of the [O III] $\lambda\lambda 4959, 5007$ lines. Thanks to the excellent sensitivity of the SDSS spectroscopic surveys, this is by far the deepest search for PNe ever taken, reaching a surface brightness of the [O III] $\lambda 5007$ line down to about 29.0 magnitude arcsec⁻². The search leads to the recovery of 13 previously known PNe in the Northern and Southern Galactic Caps. In total, 44 new planetary nebula (PN) candidates are identified, including 7 candidates of multiple detections and 37 candidates of single detection. The 7 candidates of multiple detections are all extremely large (between 21' and 154') and faint, located mostly in the low Galactic latitude region and with a kinematics similar to disk stars. After checking their images in H α and other bands, three of them are probably H II regions, one is probably associated with a new supernova remnant, another one is possibly a true PN, and the remaining two could be either PNe or supernova remnants. Based on sky positions and kinematics, 7 candidates of single detection probably belong to the halo population. If confirmed, they will increase the number of known PNe in the Galactic halo significantly. All the newly identified PN candidates are very faint, with a surface brightness of the [O III] $\lambda 5007$ line between 27.0 – 30.0 magnitude arcsec⁻², very challenging to be discovered with previously employed techniques (e.g. slitless spectroscopy, narrow-band imaging), and thus may greatly increase the number of "missing" faint PNe. Our results demonstrate the power of large scale fiber spectroscopy in hunting for ultra-faint PNe and other types of emission line nebulae. Combining the large spectral databases provided by the SDSS and other on-going projects (e.g. the LAMOST Galactic surveys), it is possible to build a statistically meaningful sample of ultra-faint, large, evolved PNe, thus improving the census of Galactic PNe.

Key words: (*ISM*): planetary nebulae: general – techniques: spectroscopic

1 INTRODUCTION

Planetary nebulae (PNe) represent the last stages of evolution for low- and intermediate-mass stars of masses less than about 8 solar masses. The PN phase begins when the central contracting white dwarf reaches an effective temperature of above 30,000 K and starts to ionize the gaseous envelope ejected during the previous Asymptotic Giant Branch (AGB) phase. The PN phase is short, lasting for just tens of thousands years maximally. PNe enrich the interstellar medium (ISM) with dust grains, helium, carbon, nitrogen,

oxygen and other products of nucleosynthesis, and are vital probes of the stellar nucleosynthesis processes, abundance gradients and chemical evolution of galaxies. In addition, PNe play a key role in studying the physics and time-scales of mass-loss and stellar evolution for low- and intermediate-mass stars (Iben 1995). PNe may also be progenitors of Type Ia supernovae that return large amounts of iron to the ISM.

New PNe have been continually discovered via various surveys (Parker et al. 2012). The Strasbourg-ESO Catalog of Galactic Planetary Nebulae (SECGPN) compiled by Acker et al. (1994, 1996) contains $\sim 1,500$ true, probable or possible PNe. Kohoutek (2001) lists $\sim 1,500$ objects classified as Galactic PNe known up to the end of 1999, as well as a number of possible pre-PNe and post-PNe. Using the

* LAMOST Fellow

† E-mail: yuanhb4861@pku.edu.cn

the Anglo-Australian Observatory UK Schmidt Telescope (AAO/UKST) SuperCOSMOS H α Survey (SHS; Parker et al. 2005), Parker et al. (2006) and Miszalski et al. (2008) present $\sim 1,200$ newly discovered true, possible or likely Galactic PNe in the Macquarie/AAO/Strasbourg H-Alpha Planetary Nebula Catalogue (MASH) and its supplement (MASH-II). From the Isaac Newton Telescope (INT) Photometric H α Survey (IPHAS; Drew et al. 2005), Viironen et al. (2009a, b) discover several PN candidates. Jacoby et al. (2010) describe a technique to search for additional unknown PNe via visually inspecting the existing data collections of the digital sky surveys (DSS) such as the POSS-I and POSS-II surveys, and find tens of new PNe. Up to now, there are in total less than 2,850 true or probable PNe known in the Milky Way (Miszalski et al. 2012). However, the number is still a small fraction of the total predicted by any PN population model. For example, the stellar population synthesis models of Moe & De Marco (2006) predict a total number of $46,000 \pm 13,000$ PNe with radii ≤ 0.9 pc in the Milky Way if all low- and intermediate-mass stars of 1 - 8 solar mass will go through a PN phase. The number drops to $\sim 6,600$ if all PNe have to form via the channel of close binaries (through the common envelope phase) (De Marco & Moe 2005). Observationally, based on a solar neighborhood (≤ 2 kpc) sample of about 200 PNe, Frew (2008) estimates a total Galactic population of $24,000 \pm 4,000$ PNe of radii ≤ 1.5 pc, or $13,000 \pm 2,000$ PNe of radii ≤ 0.9 pc.

A variety of multi-waveband observations ranging from the radio up to the X-ray have been utilized to detect PNe. Essentially, all the efforts have been based on the technique of wide field, interference filter or objective prism slitless spectroscopic imaging surveys, primarily searching for emission in the light of the [O III] $\lambda 5007$ line and/or H α . However, it is a very challenging task to find all PNe in the Galaxy directly. Firstly, since most PNe are distributed in the Galactic plane where dust extinction is high, a large fraction of them are unobservable at optical wavelengths where PNe are most luminous. Secondly, when only imaging data are available, it is difficult to differentiate PNe from other diffuse emission line nebulae such as H II regions, supernova remnants, nova shells, symbiotic nebulae and distant emission line galaxies.

The Sloan Digital Sky Survey (SDSS; York et al. 2000) provides uniform and contiguous imaging photometry for about one-third of the sky in the u, g, r, i and z bands, as well as over two million high quality low resolution optical spectra of stars, galaxies and quasars. The latest SDSS Data Release 9 (DR9; Ahn et al. 2012) delivers spectra for about 1.46 million galaxies, 0.23 million quasars and 0.67 million stars. The SDSS observations mainly target high Galactic latitude regions of the Northern and Southern Galactic Caps. If by chance a PN (or an extended emission line nebula of other types) falls in the sightline of some SDSS targets (including sky background targets by sky fibers), lines emitted by the nebula, such as the [O III] $\lambda\lambda 4959, 5007$, typically the strongest for a medium to high excitation nebula, will appear in the spectra of those targets. Then by systematically searching and measuring the [O III] $\lambda\lambda 4959, 5007$ emission lines of Galactic nebular origins in those millions of SDSS spectra, one may expect to discover and study previously unknown PNe or other types of extended emission line nebula in the Galaxy. This spectroscopic approach has the fol-

lowing advantages: a) Compared to previously commonly used techniques, such as narrow-band imaging and slitless objective prism imaging spectroscopy, the sky background is much reduced in slit or fiber spectroscopy. Thus the latter is much more sensitive to faint nebular emission and capable of detecting large (evolved and/or nearby) PNe of very low surface brightness; b) With spectral information available over a wide wavelength coverage, it is much easier to differentiate different types of emission line nebulae; and c) With a contiguous and uniform coverage over a huge sky area such as that provided by the SDSS, it is possible to construct a statistically meaningful sample to improve the census of Galactic PNe.

In this paper, we present results of a systematic search for PNe in the SDSS spectroscopic database. The paper is organized as following. In Section 2, we introduce the data and method used to search for PNe. The results are presented in Section 3 and discussed in Section 4. A brief summary then follows in Section 5.

2 DATA AND METHOD

2.1 Data

We used the SDSS DR7 (Abazajian et al. 2009) spectroscopic database in the current work. The release contains over 1.6 million low-resolution ($R \sim 1,800$) spectra targeting approximately 930,000 galaxies, 120,000 quasars, 460,000 stars and 97,000 blank sky positions. Most targets are within a large contiguous area over $7,350 \text{ deg}^2$ in the Northern Galactic Cap, with the remaining ones from a number of stripes in the Southern Galactic Cap and a few stripes across the Galactic plane targeted by the program of the Sloan Extension for Galactic Understanding and Exploration (SEGUE; Yanny et al. 2009).

Spectroscopic observations of the SDSS are usually undertaken in non-photometric conditions when the imaging camera is not in use. At least three fifteen-minute exposures are taken until the cumulative mean signal-to-noise ratio (SNR) per pixel exceeds 4 for a fiducial fiber magnitude of $g = 20.2$ and $i = 19.9$. For faint SEGUE plates, a total exposure time of about 1.5 hours is required. A total number of 640 spectra are collected simultaneously covering $3,800 - 9,200 \text{ \AA}$, at a spectral resolution of $\sim 1,800$. The large aperture size of the SDSS telescope (2.5 meter) and the long exposures (≥ 45 minutes) make the SDSS spectra extremely sensitive to narrow nebular emission lines. Note that each SDSS fiber samples a sky area of angular diameter of $3''$ and the SDSS wavelength scale is based on vacuum wavelengths.

2.2 Method

For each spectrum from the SDSS DR7 spectroscopic database, we have performed Gaussian fitting to the [O III] $\lambda\lambda 4959, 5007$ lines around their rest wavelengths. The two lines are fitted independently. To reduce the degrees of freedom of fit, we have adopted a fixed line width of FWHM 2.82 \AA and assumed a flat continuum in the vicinity of both lines. When a positive signal is detected, the SNR of the detection is then computed by dividing the peak value

of the fitted Gaussian by the standard deviation of a segment spectrum of a wavelength span of 40 Å around the rest wavelength of the line. Note that the SNRs thus calculated are lower limits of the true values. In cases of very strong signals, the SNRs would be greatly under-estimated.

To minimize spurious detections, we require that: a) SNRs of the [O III] λ5007 line should be higher than 3; b) The difference of radial velocities deduced from the two [O III] λλ4959, 5007 lines must be smaller than 60 km s⁻¹; c) The intensity ratio of the two lines F_{5007}/F_{4959} must fall between 2 and 4, bracketing the intrinsic ratio of 2.98 (Mathis & Liu 1999; Storey & Zeppen 2000). The [O III] λ5007 line emission from Galactic PNe may be contaminated by emission lines (e.g. the [O II] λλ3726, 3729 lines, the Balmer lines and the [O III] λλ4959, 5007 lines) of target galaxies and quasars. Such cases are also carefully avoided by visual check of the SDSS images and spectra to remove nearby galaxies whose [O III] emission lines are regarded as Galactic emission and distant galaxies and quasars that have an emission line shifted to the wavelength of the [O III] λ5007 line. Faint background emission line galaxies at a given redshift, such as [O II] emission line galaxies at redshift about 0.35 and Lyα emitters at redshift about 3.1, are important contaminations for PNe surveys beyond the Milky Way (e.g. Gerhard 2006 and references therein). To further avoid such contaminations, we have excluded a few PN candidates whose [O III] λ5007 line widths are larger than 4.23 Å (1.5 times the expected line width). These measures have lessened the extragalactic contamination in our work. The radial velocities of the PN candidates (see Fig. 14 in Section 4) also suggest their Galactic origins, as extragalactic origins would result a uniform radial velocity distribution. In addition, we find a few cases that some spectral features of a normal galaxy at a given redshift, such as the 4661Å feature at redshift around 0.074 and the 4819Å feature at redshift about 0.039, can mimic the [O III] λ5007 emission. Such cases are also excluded.

Detection of the [O III] λλ4959, 5007 lines is a good indication but not sufficient to identify a PN. The PN candidates found in this work may be contaminated by reflection nebulae, diffuse ionized gas, H II regions, supernova remnants, emission line stars and nova shells (Frew & Parker 2010). Imaging data, particularly narrow-band images, can provide important clues to classify the PN candidates. Therefore, both the SDSS spectra and available imaging data are used to help classify the nature of the PN candidates in this work.

3 RESULTS

After applying the above criteria, a total number of 160 spectra with reliable detections of the Galactic [O III] λλ4959, 5007 emission lines are selected. The spectral sequence number, SDSS spectral ID, the type, redshift and equatorial and Galactic coordinates of the target, the surface brightness and radial velocity of the detected Galactic [O III] λ5007 line of each spectrum are listed in Tab. 1. Note the redshifts here indicate the SDSS targets and are given by the SDSS pipeline. While the radial velocities are associated the PNe or PN candidates and measured from the [O III] λ5007 emission lines in this work. The SDSS spectra and colour-composite

thumbnails are displayed in Figs. A1 and A2 in the Appendix, respectively. Based on the coordinates and radial velocities, they are divided into 58 groups, with each group representing a PN (candidate). After cross-correlating with existing PN catalogs including SECGPN, MASH, MASH-II, Kohoutek et al. (2001) and the IPHAS PN catalog, the 58 groups are further divided into 3 categories: previously known PNe or other types of emission line nebulae recovered in this work (Spectral sequence number SEQ 1 – 37), PN candidates of multiple [O III] λ5007 detections (SEQ 38 – 123) and PN candidates of single detection (SEQ 124 – 160), with each category having 14, 7 and 37 members, respectively. Their Galactic distribution is shown in Fig. 1.

As listed in Tab. 1, the 160 SDSS spectroscopic targets include 59 galaxies (GAL), 28 blank skies (SKY), 16 blue horizontal-branch stars (BHB), 12 F-turnoff stars (FTO), 7 quasars (QSO), 9 white dwarfs (WD), 7 X-ray sources from the ROSAT All-Sky Survey (ROS; Voges et al. 1999), 7 G-dwarfs (GD), 3 hot stars (Hot), plus a few other types of object. Note that the target types are assigned by the SDSS. The fraction of spectra with detectable Galactic [O III] line emission are 0.007, 0.004, 0.006 and 0.016 per cent for target type GAL, QSO, GD and FTO, respectively. The fractions increase to 0.022, 0.025 and 0.022 per cent for target type ROS, BHB and SKY, and further to 0.087 and 0.12 for Hot and WD, respectively. Such increases are caused by the facts that it is easier to detect the [O III] λλ4959, 5007 emission on spectra of blue stars or blank skies and some of the WDs and hot stars are exactly the central stars of the PNe.

3.1 Previously known PNe

Thirteen previously known PNe (IC 4593, NGC 6210, A 39, H 4-1, K 1-16, BE UMa, NGC 3587, A 28 JnEr 1, HDW 7, A 31, EBG 6 and LoTr 5) are recovered in this work. They are all cataloged in the SECGPN catalog except for LoTr 5, which is from Kohoutek et al. (2001). Their standard PNG identifications, names, angular sizes and heliocentric radial velocities if available are listed in Tab. 1. Note that the faint low-excitation nebula PHL 932 in the SECGPN catalog, which in fact is a small H II region around a subdwarf B star (Frew et al. 2010), is also recovered. This group of PNe range widely in sizes, from compact ones of a few arcsec to very large ones of about 1,000". The radial velocities measured in this work agree well with those in the literature. Four of the known PNe are only detected in one SDSS spectrum, by marginally detected signals only for 1 of them (corresponding to a [O III] λ5007 line surface brightness S_{5007} about 28.0 magnitude arcsec⁻²). The results demonstrate the reliability and sensitivity of the current method. SDSS true-color (g, r, i) images centered at the positions of the 13 PNe are displayed in Fig. 2. They are clearly visible on those images except for BE UMa (G144.8+65.8), A 28 (G158.8+37.1), EBG 6 (G221.5+46.3) and LoTr 5 (G339.9+88.4). For the latter 4 PNe, the measured S_{5007} values are mostly around 27.0 magnitude arcsec⁻². However, they are all visible in the SDSS g -band images after rebinning (10" per pixel).

Representative spectra for each of the recovered PNe and the spatial distribution of SDSS fibers leading to their discovery are shown in the first 13 panels of Figs. 3, 4, respectively. Note that the halo PN H 4-1 was selected as a quasar candidate by the SDSS due to its very blue colors.

Table 1. List of SDSS targets whose spectra show detectable [O III] $\lambda\lambda 4959, 5007$ emission from Galactic PNe, H II regions and PN candidates.

SEQ	Spectr. ID ^a	Type ^b (Initial)	Redshift	RA (J2000.0)	Dec (J2000.0)	l	b	S ₅₀₀₇ ^c	Vr (km s ⁻¹)
Recovered PNe and H II regions									
PN G025.3+40.8, IC 4593, 13'', 22.0 km s ⁻¹									
1 ^d	54569-2527-241	GAL	0.07275	242.91496	12.04709	25.29303	40.84380	28.13	24.4
PN G043.1+37.7, NGC 6210, 16.2'', -36.2 km s ⁻¹									
2 ^d	53135-1414-173	GAL	0.04877	251.23384	23.77270	43.11331	37.65422	28.19	-57.0
3 ^d	53135-1414-174	MD	-0.00038	251.16985	23.70874	43.01453	37.69176	28.36	-37.1
4 ^d	53135-1414-176	GAL	0.20437	251.09543	23.76732	43.06049	37.77392	26.67	-40.5
5 ^d	53135-1414-194	GAL	0.43010	251.05946	23.77403	43.05658	37.80737	27.40	-47.6
6 ^d	53135-1414-198	FTO	2.19684	251.07339	23.78899	43.07936	37.79949	27.13	-39.2
PN G047.0+42.4, A 39, 174.0''									
7	52822-1408-528	GAL	0.13308	246.88931	27.88820	47.02350	42.47912	23.16	3.0
8 ^d	52822-1408-536	QSO	-0.00038	246.86891	27.92838	47.07146	42.50535	27.62	13.5
9	53149-1421-253	GAL	0.13302	246.87674	27.91645	47.05768	42.49604	24.14	5.3
PN G049.3+88.1, H 4-1, 2.7'', -141.0 km s ⁻¹									
10 ^e	54156-2241-108	QSO	-0.00062	194.86575	27.63631	49.30931	88.14751	18.14 ^f	-184.8 ^f
PN G094.0+27.4, K 1-16, 114.0''									
11	54630-2552-347	WD	0.18159	275.46713	64.36484	94.02541	27.42847	24.65	-58.6
12	54632-2552-347	WD	-0.00007	275.46713	64.36484	94.02541	27.42847	24.65	-57.2
H II region, PHL 932, 275.0''									
13 ^g	51821-0421-369	GAL	-0.00003	14.97583	15.73003	125.92473	-47.09252	28.33	-10.5
PN G144.8+65.8, BE UMa									
14	52412-0968-054	GAL	0.07743	179.43967	48.92075	144.82858	65.86246	27.08	-83.6
15	52412-0968-060	QSO	4.24529	179.49153	48.94882	144.72203	65.85540	27.94	-127.0
PN G148.4+57.0, NGC 3587, 170.0'', 6.0 km s ⁻¹									
16 ^d	52649-1012-449	QSO	1.18744	168.76855	55.02877	148.42288	57.06946	26.15	-9.5
17	52649-1012-405	GAL	0.00007	168.68710	55.03819	148.47510	57.03123	21.26	1.1
18 ^d	52649-1012-406	GAL	-0.00002	168.62302	55.01423	148.55469	57.02437	25.80	-6.6
19	52707-1013-340	GAL	-0.00001	168.69135	55.00916	148.50752	57.05441	20.46	-0.7
PN G158.8+37.1, A 28, 270.0'', -2.0 km s ⁻¹									
20	54425-1784-532	HOT	-0.00006	130.39819	58.23010	158.80217	37.17947	26.91	-8.2
PN G164.8+31.1, JnEr 1, 380.0'', -84 km s ⁻¹									
21	53383-1870-464	GAL	-0.00028	119.42754	53.44424	164.77774	31.16045	24.13	-53.9
22	53383-1870-465	GAL	-0.00027	119.42459	53.40979	164.81770	31.15596	24.91	-71.5
23	53383-1870-466	GAL	-0.00022	119.40196	53.43252	164.78998	31.14433	24.44	-66.0
PN G211.4+18.4, HDW 7, 94.0''									
24	54505-2945-483	WD	0.00058	118.79710	9.55256	211.46860	18.46137	25.19	60.1
PN G219.1+31.2, A 31, 970.0'', 41.0 km s ⁻¹									
25	53086-1760-021	GAL	0.06295	133.63991	8.87866	219.19708	31.35715	26.37	25.9
26	53086-1760-023	GAL	0.06407	133.48776	8.79611	219.20520	31.18578	26.80	20.3
27	53086-1760-026	GAL	0.06426	133.62056	8.74568	219.32645	31.28074	27.62	2.3
28	53086-1760-029	GAL	0.07250	133.56465	8.85769	219.18030	31.28123	24.71	38.3
29	53086-1760-031	SKY	*****	133.57205	8.92268	219.11600	31.31669	24.38	35.6
30	53086-1760-034	GAL	0.06387	133.56229	8.98637	219.04419	31.33636	26.49	20.6
31	53086-1760-038	QSO	1.64963	133.53564	8.90037	219.12065	31.27456	24.26	35.8
32	53086-1760-039	GAL	0.17061	133.48769	8.90032	219.09605	31.23210	25.35	35.1

^a In format mjd-plateid-fiberid.^b GAL: galaxy; MD: M-dwarf; FTO: F-turnoff star; QSO: quasar; WD: white dwarf; HOT: hot star; ROS: ROSAT source; GD: G-dwarf; BHB: blue horizontal branch star; KG: K-giant; SER: hand-selected target.^c Using the definition by Jacoby (1989): $m_{5007} = -2.5 \log(F_{5007}) - 13.74$. $S_{5007} = m_{5007} + 2.5 \log(\pi \times r^2)$, $r = 1.5''$ is the SDSS fiber radius.^d Indicating haloes of PNe.^e Indicating halo PNe and PN candidates.^f Based on [O III] $\lambda 4959$ line. The [O III] $\lambda 5007$ line of this target is partly clipped as cosmic ray.

Table 1. – continued

SEQ	Spectr. ID ^a	Type ^b (Initial)	Redshift	RA (J2000.0)	Dec (J2000.0)	l	b	S ₅₀₀₇ ^c	Vr (km s ⁻¹)
PN G221.5+46.3, EGB 6, 720.0''									
33	54153-2584-288	GAL	0.10275	148.24554	13.75261	221.57625	46.36752	27.92	-30.2
34	54153-2584-297	GAL	0.24429	148.22514	13.75945	221.55511	46.35248	27.42	0.2
PN G339.9+88.4, LoTr 5, 525.0''									
35	54505-2661-581	SKY	*****	193.89409	25.84894	339.06198	88.42075	25.07	-13.6
36	54505-2661-585	GAL	0.08507	193.90659	25.92518	341.07626	88.47519	25.42	-11.6
37	54505-2661-587	GAL	0.36823	193.87260	25.87905	339.13062	88.45647	25.56	2.4
PN candidates of multiple detections									
PN? G055.9-3.9, ≥ 45', 11.8 km s ⁻¹									
38	53679-2338-256	SKY	*****	297.74210	18.17833	55.88768	-4.29661	30.09	14.0
39	53679-2338-284	SKY	*****	297.34210	18.27833	55.78187	-3.91819	28.64	14.6
40	53679-2338-318	SKY	*****	297.24210	18.77833	56.16679	-3.58433	28.99	7.0
PN? G070.8+10.4, ≥ 111', 1.4 km s ⁻¹									
41	54393-2821-361	ROS	-0.00054	289.77692	38.71134	70.66661	11.62647	28.95	-1.6
42	54393-2821-412	SKY	*****	290.07880	38.68260	70.74431	11.40165	29.65	4.4
43	54393-2821-542	GD	-0.00042	291.34879	38.40768	70.93838	10.38881	29.59	7.8
44	54393-2821-544	FTO	-0.00023	291.22098	38.30778	70.80202	10.43398	29.78	-7.7
45	54393-2821-621	GD	-0.00039	292.08890	38.30058	71.10625	9.82225	28.79	4.3
PN? G108.9+10.7, ≥ 48', 10.2 km s ⁻¹									
46	53917-2537-356	ROS	-0.00023	330.17175	69.56667	108.95517	11.47278	26.96	4.6
47	53915-2545-307	ROS	-0.00027	331.29926	68.88441	108.85572	10.68802	27.93	21.4
48	53915-2545-309	ROS	-0.00026	331.40918	68.89623	108.89516	10.67371	28.06	4.5
PN? G117.1-26.3, ≥ 85', 17.7 km s ⁻¹									
49	52999-1468-026	BHB	-0.00033	6.51919	35.14665	117.09232	-27.43737	27.68	5.5
50	52999-1468-531	BHB	-0.00026	5.30235	36.17010	116.13050	-26.30212	29.11	30.0
PN? G126.8-15.5, ≥ 21', -25.3 km s ⁻¹									
51	52883-1471-581	BHB	-0.00034	18.40656	47.04016	126.85489	-15.66251	28.56	-29.8
52	52883-1471-585	BHB	-0.00050	18.42049	47.13765	126.85564	-15.56457	27.85	-30.0
53	52883-1471-587	BHB	-0.00020	18.25561	47.14178	126.73930	-15.57034	26.93	-36.4
54	52883-1471-589	BHB	-0.00037	18.24209	46.98835	126.74360	-15.72399	28.94	-27.4
55	52883-1471-601	BHB	-0.00034	18.40916	47.29352	126.83323	-15.41001	27.37	-15.7
56	52913-1472-581	BHB	-0.00033	18.51901	47.23272	126.91594	-15.46383	27.87	-23.4
57	52913-1472-584	BHB	-0.00040	18.22545	47.24541	126.70879	-15.46887	28.31	-24.2
58	52913-1472-613	BHB	-0.00033	18.27040	47.27103	126.73801	-15.44070	27.91	-15.4
PN? G202.0+19.8, ≥ 154', 13.3 km s ⁻¹									
59	53437-2074-058	KG	0.00065	116.29646	17.47382	202.77744	19.52307	28.11	14.4
60	53437-2074-115	SKY	*****	116.47591	17.79686	202.53384	19.80765	29.25	1.2
61	53437-2074-144	SKY	*****	116.26263	17.76538	202.47964	19.60857	27.92	3.4
62	53437-2074-156	BHB	0.00098	116.16776	18.06075	202.15363	19.64182	28.23	18.3
63	53437-2074-158	GD	0.00018	116.21307	18.08687	202.14609	19.69169	28.01	8.8
64	53437-2074-441	SKY	*****	116.02364	19.24729	200.93568	19.97874	28.57	-16.0
65	53437-2074-451	GD	0.00021	116.11795	19.04743	201.16847	19.98346	28.85	12.1
66	53437-2074-453	LOW	-0.00016	116.05990	18.97441	201.21741	19.90454	28.12	36.8
67	53437-2074-454	FTO	-0.00003	115.99590	19.23490	200.93706	19.94979	28.89	5.9
68	53437-2074-459	WD	0.00015	116.12531	18.88782	201.32784	19.92792	28.17	17.0
69	53437-2074-486	GD	0.00003	116.06538	18.42509	201.75722	19.69521	28.78	22.2
70	53437-2074-494	FTO	0.00025	116.19690	18.25080	201.97949	19.74185	28.29	6.4
71	53437-2074-500	SKY	*****	116.19335	18.59982	201.63664	19.87516	28.15	13.9
72	53437-2074-518	SKY	*****	116.25914	18.23840	202.01624	19.79138	28.31	8.7
73	54495-2890-089	SKY	*****	116.31457	17.21025	203.04138	19.43450	28.62	38.8
74	54495-2890-516	FTO	-0.00037	116.19057	18.45045	201.78175	19.81443	27.81	14.2
75	54495-2890-519	BHB	-0.00011	116.18020	18.42692	201.80069	19.79618	27.88	5.9
76	54495-2890-520	SKY	*****	116.26186	18.37812	201.88063	19.84842	28.67	21.4
77	54497-2915-041	BHB	0.00031	116.28696	16.97946	203.25475	19.31854	28.40	18.1
78	54497-2915-056	ROS	0.00022	116.29904	17.16793	203.07632	19.40408	28.34	33.8
79	54497-2915-059	LOW	0.00028	116.27701	17.50570	202.73859	19.51864	27.74	19.8
80	54497-2915-086	BHB	2.26947	116.23821	17.50462	202.72411	19.48423	28.14	9.0

Table 1. – *continued*

SEQ	Spectr. ID ^a	Type ^b (Initial)	Redshift	RA (J2000.0)	Dec (J2000.0)	l	b	S ₅₀₀₇ ^c	Vr (km s ⁻¹)
81	54497-2915-108	LOW	-0.00009	116.49316	17.72202	202.61385	19.79330	28.70	56.9
82	54497-2915-111	SKY	*****	116.31377	17.96962	202.30058	19.73370	28.71	6.6
83	54497-2915-114	BHB	0.00052	116.38711	18.19564	202.10867	19.88648	29.15	-4.7
84	54497-2915-143	GD	0.00007	116.21307	18.08687	202.14609	19.69169	27.87	6.1
85	54497-2915-146	WD	-0.00008	116.23761	17.85658	202.38068	19.62261	27.88	11.8
86	54497-2915-149	BHB	2.54176	116.25659	17.87834	202.36699	19.64778	27.76	-7.0
87	54497-2915-155	ROS	0.00029	116.19150	18.01605	202.20670	19.64501	28.18	16.5
88	54497-2915-156	LOW	-0.00015	116.23810	17.76487	202.47035	19.58691	28.08	36.7
89	54497-2915-159	SKY	*****	116.11637	17.94356	202.24760	19.55080	28.61	10.8
90	54497-2915-406	WD	0.00029	115.97432	19.42876	200.73845	20.00597	28.86	-8.5
91	54497-2915-411	SKY	*****	115.99598	19.19868	200.97261	19.93584	28.39	26.4
92	54497-2915-417	SKY	*****	115.92066	19.49002	200.65753	19.98295	28.81	-13.2
93	54497-2915-456	WD	0.00013	116.12531	18.88782	201.32784	19.92792	27.83	3.5
94	54497-2915-457	LOW	-0.00018	116.05990	18.97441	201.21741	19.90454	28.35	36.5
95	54497-2915-508	FTO	0.00042	116.19148	18.38159	201.84947	19.78831	27.84	5.5
96	54497-2915-519	SKY	*****	116.19062	18.53694	201.69713	19.84825	27.71	15.5
97	54497-2915-520	SKY	*****	116.21683	18.51275	201.73111	19.86169	28.21	7.0
PN? G247.7+47.8, $\geq 103'$, -0.2 km s ⁻¹									
98	51957-0273-023	GAL	0.31444	159.04120	-0.36577	247.57170	47.43261	27.30	-8.9
99	51957-0273-026	SKY	*****	159.12874	-0.40942	247.70717	47.46691	26.87	8.1
100	51957-0273-028	GAL	0.28128	159.12106	-0.34738	247.63229	47.50360	26.94	1.1
101	51957-0273-029	GAL	0.28226	159.12099	-0.32535	247.60834	47.51856	26.48	8.4
102	51957-0273-031	GAL	0.19159	159.26550	-0.35509	247.78667	47.60394	27.41	3.7
103	51957-0273-074	GAL	0.08492	158.97260	-0.32811	247.46193	47.40798	27.86	-5.5
104	51957-0273-624	SKY	*****	159.19664	0.19700	247.11470	47.92880	28.54	10.4
105	51957-0273-632	QSO	2.68057	159.29083	0.04310	247.37874	47.89370	27.31	4.1
106	51913-0274-235	GAL	0.13274	159.76680	-0.03093	247.94521	48.19136	28.82	39.9
107	51913-0274-245	GAL	0.07414	159.29501	-0.69016	248.17795	47.39594	27.94	-9.6
108	51913-0274-260	GAL	0.13560	159.31465	-0.68561	248.19299	47.41333	28.48	12.7
109	51913-0274-262	GAL	0.13041	159.42221	-0.29270	247.87813	47.76096	27.92	-4.0
110	51913-0274-264	GAL	0.19021	159.54897	-0.32973	248.04750	47.82798	28.12	3.9
111	51913-0274-269	QSO	1.49792	159.44756	-0.27887	247.88890	47.78891	27.83	-3.3
112	51913-0274-271	GAL	0.22292	159.49477	-0.09606	247.73804	47.94829	27.78	-18.4
113	51913-0274-272	GAL	0.09643	159.41495	-0.18049	247.74878	47.83232	27.73	0.2
114	51913-0274-275	GAL	0.12643	159.56216	0.01032	247.69055	48.07015	28.21	-4.2
115	51913-0274-279	SKY	*****	159.54359	-0.29257	248.00169	47.84953	27.92	15.6
116	51913-0274-280	GAL	0.13166	159.42281	-0.02235	247.58429	47.94593	27.93	-12.1
117	51913-0274-303	AGB	0.00011	159.14861	-0.01012	247.29315	47.75314	28.42	-31.6
118	51913-0274-308	GAL	0.11394	159.34489	-0.51348	248.03841	47.55344	28.28	-11.4
119	51913-0274-317	GAL	0.34924	158.99289	-0.37309	247.53102	47.39225	28.08	0.6
120	51913-0274-352	GAL	0.09614	159.39848	0.42168	247.07143	48.22945	28.00	0.4
121	51913-0274-395	GAL	0.04997	159.52567	0.20685	247.43771	48.17726	28.12	14.8
122	51913-0274-399	GAL	0.14091	159.71764	0.14117	247.70616	48.27310	28.07	14.8
123	51910-0275-343	SKY	*****	160.24200	0.46917	247.88557	48.88010	28.18	-35.0
PN candidates of single detection									
124	54616-2929-558	WD	-0.00027	207.65657	29.12170	45.07235	76.80797	28.34	-49.8
125	54590-2971-564	GAL	0.35333	256.99677	38.04440	61.87091	35.92686	28.70	-28.5
126	54065-2441-461	FTO	-0.00023	46.03791	38.36896	149.67056	-17.51643	27.09	36.3
127	52672-1018-099	SKY	*****	181.80371	54.01628	136.77541	61.90734	27.74	-9.2
128 ^e	52264-0739-278	GAL	0.08533	339.29327	13.27799	79.78974	-38.09938	26.54	138.5
129	54393-2821-116	ROS	-0.00121	291.05371	37.17148	69.70863	10.04544	29.68	70.2
130	53084-1348-466	QSO	0.11963	214.93448	40.80570	75.55096	67.25848	27.72	-53.3
131	52672-1207-593	HOT	0.00016	126.92689	29.63689	193.59642	32.74832	28.16	51.5
132	52876-1406-593	GAL	0.15904	243.84950	30.01589	49.22656	45.49409	27.55	9.9
133	53915-2545-120	SKY	*****	335.51306	69.08811	110.23125	9.98616	28.70	-57.9
134	53313-1864-263	HOT	0.00025	111.00721	41.05582	177.26117	23.24113	28.21	99.7
135	52998-1596-413	GAL	0.14350	149.43852	38.02654	184.97514	52.19475	28.27	53.9
136 ^e	52254-0693-309	GAL	0.14597	14.01955	-0.07452	125.48116	-62.92331	28.48	124.4
137	53384-2040-362	FTO	-0.00067	18.66322	26.55484	129.35364	-36.02728	27.35	-36.2
138	54271-2449-254	FTO	-0.00095	231.37177	48.91985	79.77677	53.25694	28.15	-92.1
139	53389-1939-591	GAL	0.04298	142.93498	29.79568	197.16505	46.36980	27.95	101.2
140 ^e	53852-2483-142	GAL	0.35430	163.60043	16.17773	228.87439	60.77887	28.39	-100.5

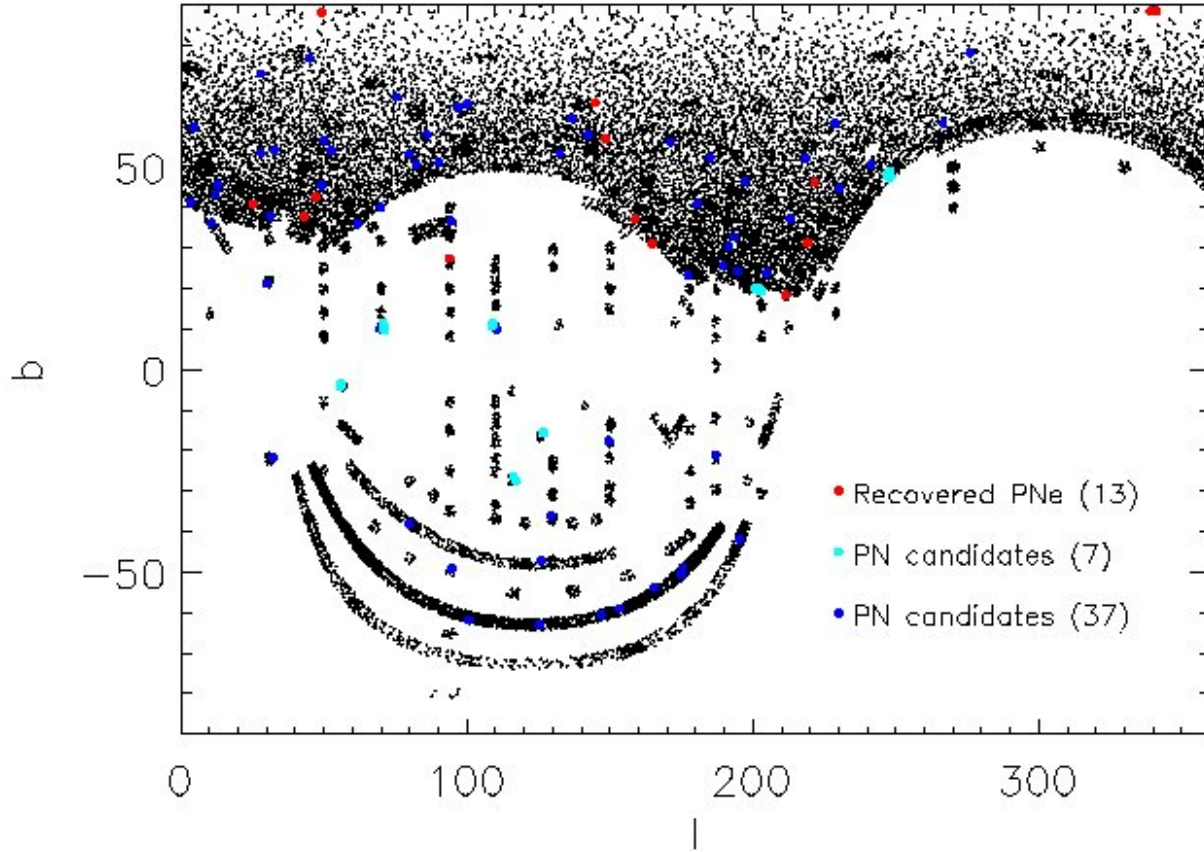


Figure 1. Galactic distribution of recovered PNe (red) within the SDSS footprint, newly discovered PN candidates of multiple detections (cyan) and of single detection (blue). Black dots show SDSS spectroscopic targets – to avoid crowiness, only 1 per cent randomly selected SDSS spectroscopic targets are shown.

Table 1. – *continued*

SEQ	Spectr. ID ^a	Type ^b (Initial)	Redshift	RA (J2000.0)	Dec (J2000.0)	l	b	S ₅₀₀₇ ^c	Vr (km s ⁻¹)
141 ^e	52823-1355-045	GAL	0.12701	234.14221	33.01287	52.58269	54.02250	27.95	125.9
142	52736-1284-567	GAL	0.08570	207.05148	49.08120	100.18240	65.46390	27.94	22.8
143 ^e	53319-1923-096	QSO	1.83425	121.25446	17.37173	204.86263	23.83992	28.29	-128.8
144	51793-0402-550	GAL	0.05973	28.03717	0.28346	153.43134	-58.94556	28.62	-110.0
145	53535-1711-423	SKY	*****	219.72304	10.35628	4.55046	59.65312	28.74	79.9
146	53437-0614-223	FTO	0.95050	229.77182	55.56635	90.17770	51.11973	28.83	-25.0
147	54539-1670-090	SKY	*****	209.47391	48.95816	96.89783	64.67480	27.95	-5.0
148	53032-1561-055	GAL	0.25434	42.94295	-0.12352	174.86002	-50.45137	29.09	-41.8
149 ^e	51994-0514-467	SKY	*****	175.95602	2.78185	266.43881	60.76971	28.69	-112.8
150	54095-2622-442	GD	-0.00019	354.50580	9.70257	94.63840	-49.09390	27.45	51.2
151	52337-0778-423	GAL	0.17002	180.33919	62.85752	132.46504	53.33398	28.21	21.4
152	51690-0345-306	GAL	0.05009	241.21989	-0.03852	10.82465	36.23080	28.61	-0.1
153 ^e	54627-2318-563	WD	-0.00038	302.02335	-10.40879	32.09501	-21.69910	28.52	147.1
154	53770-2124-193	GAL	0.06092	211.54666	24.43916	28.02714	72.97640	28.23	-103.7
155	54232-2598-135	GAL	0.11269	187.24854	16.46037	275.80475	78.13292	27.92	-8.8
156	52733-1047-622	GAL	0.15941	222.40582	49.86702	86.12347	57.95991	28.23	-35.4
157	54616-2818-084	FTO	-0.00033	262.66470	7.19039	30.17883	21.21649	29.05	42.0
158	52619-0931-310	PHO	-0.00015	123.81640	30.65392	191.61670	30.41910	27.74	92.5
159	54096-2673-541	FTO	1.02667	71.81145	11.45566	187.05783	-21.05784	29.47	92.3
160	52411-0925-557	SER	1.27697	233.76009	-1.63877	3.45333	41.25254	28.70	30.2

Its "broad" [O III] $\lambda 5007$ and $H\alpha$ emission lines are due to saturation.

The outer haloes of PNe IC 4593, NGC 6210 and NGC 3587 are also recovered, and fainter and larger than previous findings in the first two cases. IC 4593 has a bright core of $10''$ in diameter and an extended irregular outer halo of $130'' \times 120''$ (Corradi et al. 1997). Its faint halo is recovered in this work but at a larger distance of $108''$ and of $S_{5007} = 28.13$ magnitude arcsec $^{-2}$. NGC 6210 has a bright core of $12'' \times 8''$ in size, which is surrounded by a faint halo-like structure with a diameter about $20''$ (e.g. Pottasch et al. 2009). In this work we find that NGC 6210 has a much larger and fainter halo extending to a few arcmin away and of $S_{5007} \sim 27.0$ magnitude arcsec $^{-2}$. NGC 3587, also named as M 97 or Owl Nebula, is a very bright spherical PN with a diameter about $2.8'$ in the SDSS image. But it also has a surrounding halo (e.g. Kwitter, Chu & Downes 1991; Hajian et al. 1997), which is well detected at $2.6'$ away in this work.

Some known PNe and PN candidates in the SDSS footprint are missed in our search. For example, 6 PNe (G013.3+32.7, G061.9+41.3, G064.6+48.2, G208.5+33.2, G238.0+34.8 and G303.6+40.0) and 4 PN candidates (G221+45, G095+38, G275+72 and G315+59) from the SEGPN catalog and 4 objects (G144.8+65.8, G003.3+66.1, G085+52 and G052.7+50.7) from Kohoutek (2001) of Galactic latitude larger than 20° are missed. We have investigated these cases. The 6 PNe are clearly visible in the SDSS images but missed simply because there are no SDSS spectroscopic targets surrounding them. For the remaining 8 objects, they are missed because there are no SDSS spectroscopic observations, the SNRs of the [O III] $\lambda 5007$ detections are too low or they are possibly false PNe. The most oxygen-deficient halo PN TS 01 (Stasińska et al. 2010) was observed by the SDSS. However, due to its unusually low oxygen abundance and consequently extremely weak [O III] lines relative to $H\beta$, we failed to detect its [O III] $\lambda 4959$ line and missed it in the search. The result suggests that our method can effectively find true PNe if there are SDSS fibers pointing to them, but may miss unusual halo PNe such as TS 01.

3.2 PN candidates of multiple detections

Seven PN candidates of multiple (2 – 39) detections are identified based on the spatial positions and radial velocities. Each of them is assigned a PNG identification according to its median Galactic coordinates. The "?" in the PNG identifications indicates they are PN candidates which need confirmation. Their minimum sizes and average radial velocities are also estimated and given in Tab. 1. Their Galactic distribution is shown in Fig. 1. Six candidates are located in the low Galactic latitude region ($|b| \leq 30^\circ$) and discovered by the SEGUE plates. All the candidates have extremely large sizes, extending from $21'$ to $154'$.

Since the typical values of S_{5007} for these candidates are around 28.0 magnitude arcsec $^{-2}$, they are invisible on Fig. A2. Representative spectra of each newly discovered PN candidate and the spatial distribution of SDSS fibers leading to its discovery are shown in the last 7 panels of Figs. 3, 4, respectively. Based on Fig. 4 alone, we can not rule out the small possibility that the first 4 PN candidates, namely PN? G055.9–3.9, PN? G070.8+10.4, PN? G108.9+10.7 and

PN? G117.1–26.3, might be multiple PNe lying closely in the field. These PN candidates may be contaminated by diffuse ionized gas, H II regions, supernova remnants and so on (Frew & Parker 2010). It's possible to distinguish PNe from H II regions and supernova remnants based on line flux ratios (e.g. Kniazev et al. 2008; Sabin et al. 2013). However, due to the faintness of the candidates and the $H\alpha$ and $H\beta$ lines may be strongly affected by stellar absorptions, it's very difficult to classify the candidates based on line flux ratios. Each candidate has spectra that show very weak or non-detections of the $H\alpha$, $H\beta$ and [N II] $\lambda\lambda 6548, 6584$ lines relative to the [O III] $\lambda\lambda 4959, 5007$ lines, indicating that they are PN candidates. However, some candidates have spectra that show good detections of the [N II] $\lambda\lambda 6548, 6584$ lines (e.g. G055.9–3.9 and G070.8+10.4) and the [S II] $\lambda\lambda 6716, 6731$ lines (G108.9+10.7, G126.8–15.5 and G202.0+19.8), indicating that they could also be H II regions or supernova remnants.

3.3 Imaging analysis of PN candidates of multiple detections

To further investigate the nature of these PN candidates, We have checked their images from the Virginia Tech Spectral-Line Survey (VTSS; Dennison, Simonetti & Topasna 1998), the Southern H-Alpha Sky Survey Atlas (SHASSA; Gaustad et al. 2001), the Wide-field Infrared Survey Explorer (WISE; Wright et al. 2010) and the DSS. Both VTSS and SHASSA have modest angular resolution ($96''$ per pixel for VTSS and $48''$ per pixel for SHASSA) and are very deep (down to ~ 1 Rayleigh at $H\alpha$), thus very suitable to examine the large and faint PN candidates in this work. To increase the SNR, the DSS and WISE images are rebinned to $10''$ per pixel. The results are shown in Figs. 5–10.

Fig. 5 displays the VTSS continuum-corrected $H\alpha$ and WISE $W4$ images of the PN candidate G055.9–3.9. The circles indicate the positions where the [O III] $\lambda\lambda 4959, 5007$ lines are detected. The candidate is invisible in the DSS-II blue plate image. It's shown that PN? G055.9–3.9 is not a PN but part of an H II region. Fig. 6 displays the VTSS continuum-corrected $H\alpha$ image of the PN candidate G070.8+10.4. This candidate is probably not a PN but an ionized $H\alpha$ filament associated with an H II region. PN? G055.9–3.9 and PN? G070.8+10.4 are not PNe but H II regions, consistent with the fact that both candidates show good detections of the [N II] $\lambda\lambda 6548, 6584$, the [S II] $\lambda\lambda 6716, 6731$, and relatively strong $H\alpha$ and $H\beta$ to the [O III] $\lambda\lambda 4959, 5007$ lines. Fig. 7 displays the VTSS continuum-corrected $H\alpha$, WISE $W4$ and DSS-II blue plate images of the PN candidate G108.9+10.7. In the bottom-left corner of the VTSS image, there is probably a new supernova remnant (SNR? G107.1+9.0) based on its spherical morphology and filamentary structure. PN? G108.9+10.7 is probably not a PN but associated with this supernova remnant, consistent with the facts that it shows relatively strong [S II] $\lambda\lambda 6716, 6731$ emission lines and it's discovered in the spectra of ROS targets. Fig. 8 displays the VTSS continuum-corrected $H\alpha$ and DSS-II blue plate images of the PN candidate G117.1–26.3. The detected [O III] emission is probably from $H\alpha$ filaments of the diffuse ISM, as seen in the DSS-II image. Therefore, this candidate is not a PN. Fig. 9 shows the VTSS continuum-corrected $H\alpha$, WISE $W4$ and DSS-II

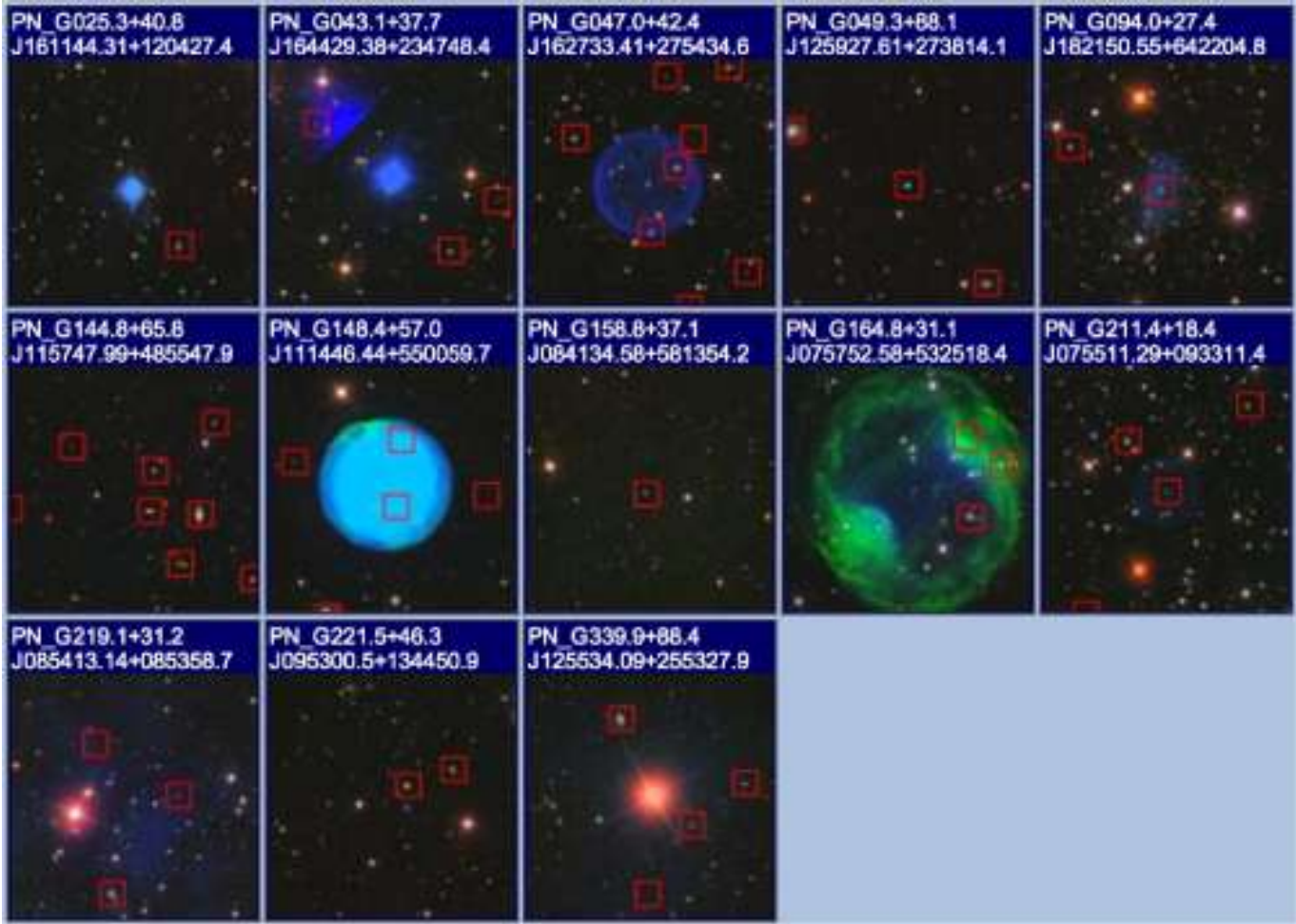


Figure 2. SDSS true-color (g , r , i) images of the 13 recovered previously known PNe. The field of view for each panel is $6' \times 6'$, north is up and east to the left. The PNG identification and field center (in Jhhmss.s+ddmss.s format) are labeled on the top of each panel. The red squares indicate SDSS spectroscopic targets.

blue plate images of the PN candidate G126.8–15.5. Based on the VTSS and WISE images, this candidate is probably a true PN. However, it also shows strong [S II] $\lambda\lambda 6716$, 6731 emission lines and could be a new supernova remnant. For PN candidate G202.0+19.8, the VTSS image is not available. It's invisible in either the WISE $W4$ or DSS-II blue plate images. Although it is covered by the Wisconsin H-Alpha Mapper Survey (WHAM; Haffner et al. 2003), the spatial resolution of WHAM data is too low (about 1°). Its arc-like morphology and the detections of strong [S II] $\lambda\lambda 6716$, 6731 emission lines suggest it's a supernova remnant. But, it could also be a normal PN that has experienced an interaction with the ISM. Deep narrow-band imaging and spectroscopic observations are needed to confirm the nature of PN? G126.8–15.5 and PN? G202.0+19.8. Fig. 10 shows the SHASSA continuum-corrected $H\alpha$, WISE $W4$ and DSS-II blue plate images of the PN candidate G247.7+47.8. The candidate is seen in all the three images and possibly a true PN, consistent with the fact that all its spectra show very weak or non-detections of the $H\alpha$, $H\beta$ and [N II] $\lambda\lambda 6548$, 6584 lines.

In summary, PN? G055.9–3.9, PN? G070.8+10.4 and PN? G117.1–26.3 are probably not PNe but H II regions,

PN? G108.9+10.7 is probably associated with a new supernova remnant, PN? G126.8–15.5 and PN? G202.0+19.8 could be either PNe or supernova remnants, and PN? 247.7+47.8. is a possible PN.

3.4 PN candidates of single detection

Thirty-seven PN candidates of single detection are found. Compared to the PN candidates of multiple detections, most PN candidates of single detection are distributed in the Northern and Southern Galactic Caps, as shown in Fig. 1. Therefore, the possibilities of contamination by H II regions and supernova remnants are relatively low. Some of them have large radial velocities, suggesting that they are probably halo PNe (see Section 4.3).

As the PN candidates of multiple detections, the candidates of single detection have S_{5007} around 28.0 magnitude arcsec^{-2} , thus invisible on Fig. A2 either. Eleven candidates have either SHASS (SEQ 136, 144, 148, 149, 152, 153, 160) or VTSS (SEQ 126, 129, 133, 159) $H\alpha$ images, as shown in Fig. 11. Based on the images, 3 candidates (SEQ 126, 129, 159) are probably H II regions, 4 candidates (SEQ 144, 148, 152, 160) seem to be around very diffuse H II re-

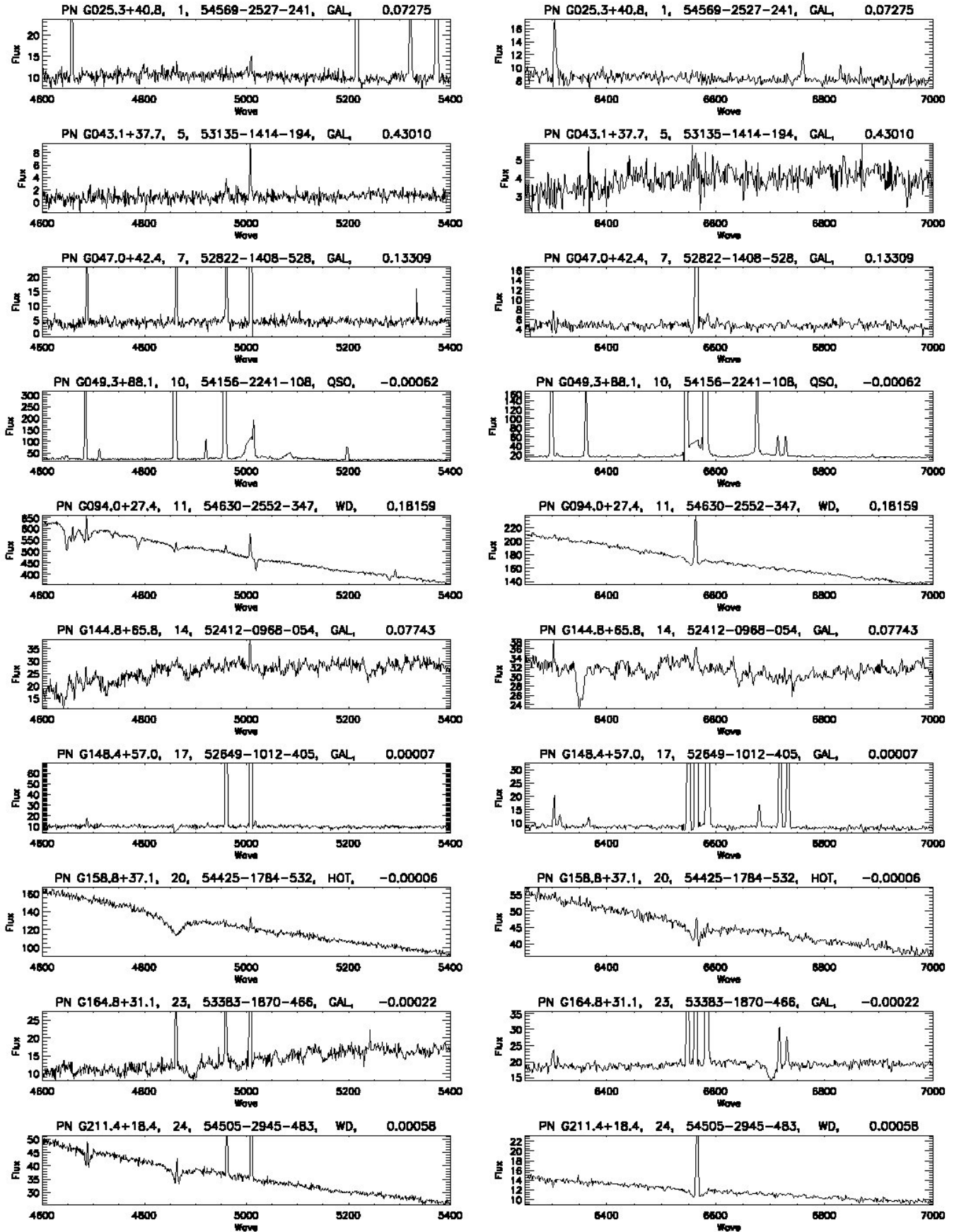


Figure 3. Examples of SDSS spectra with well detected [O III] $\lambda\lambda 4959, 5007$ lines from Galactic PNe and PN candidates. The PNG identification, SEQ, SDSS spectral ID, initial target type and redshift from Tab. 1 are labeled on the top of each panel. The wavelengths are observed values. The fluxes are in unit of $10^{-17} \text{ ergs cm}^{-2} \text{ \AA}^{-1}$.

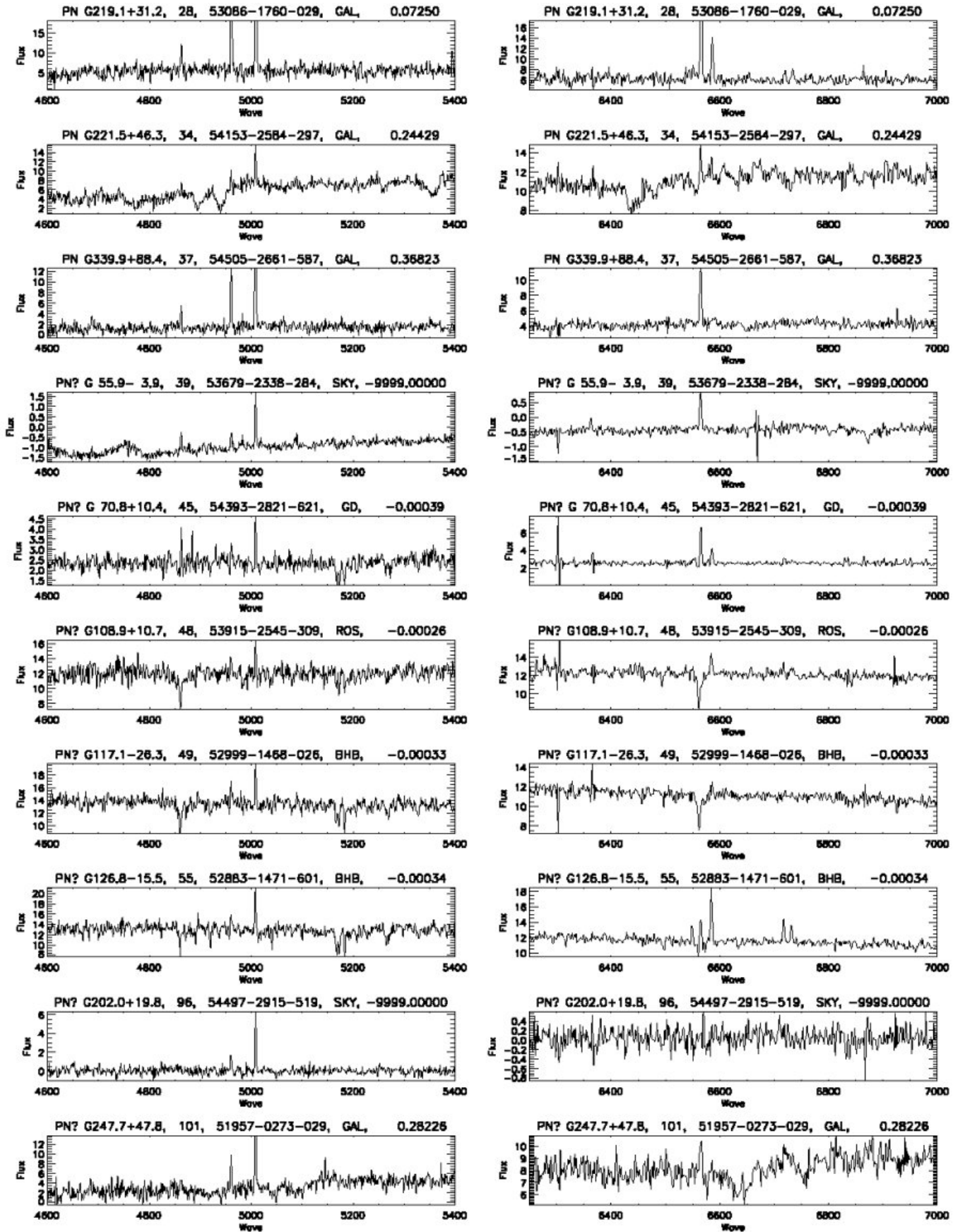


Figure 3. -continued

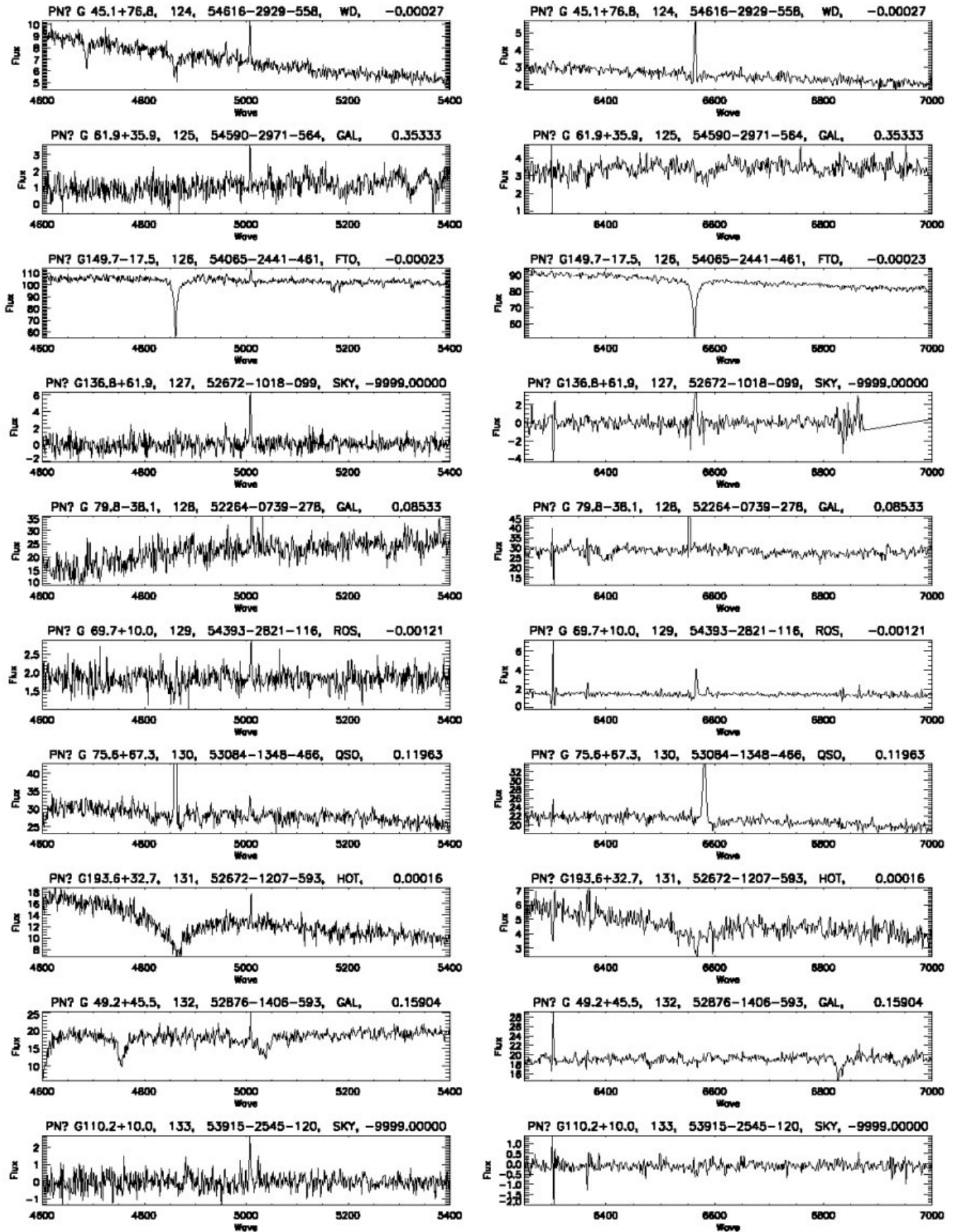


Figure 3. -continued

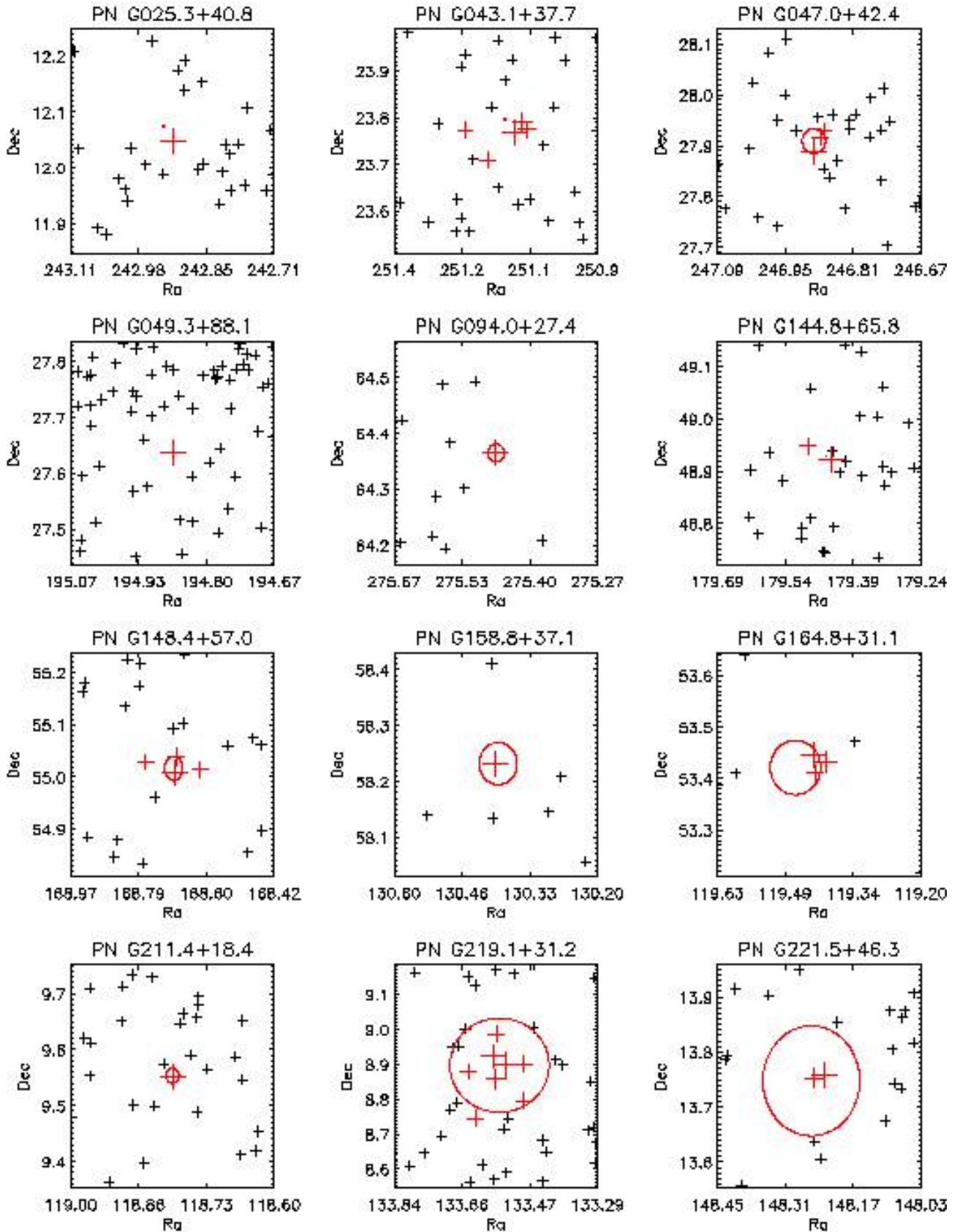


Figure 4. Spatial distribution of the targets with detectable [O III] $\lambda\lambda 4959, 5007$ lines for the 13 previously known PNe and 7 newly discovered PN candidates of multiple detections. The PNG identification is labeled on the top of each panel. The black crosses indicate SDSS spectroscopic targets. The red crosses represent the targets with detectable [O III] lines, with sizes positively and linearly correlated with line fluxes. The red circles indicate optical sizes of the known PNe. Note the size of PN G144.8+65.8 is not available from the literature.

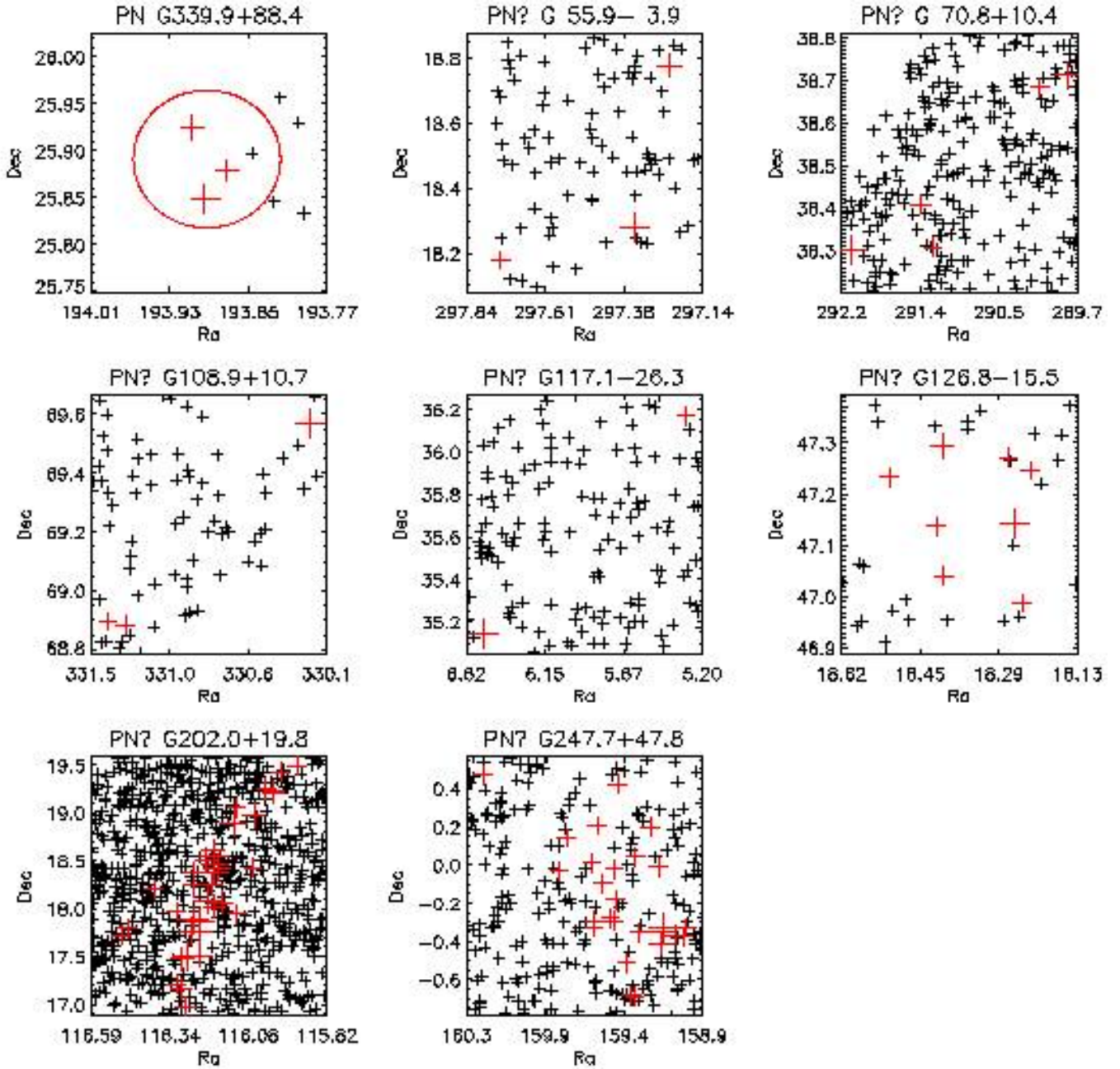


Figure 4. –*continued*. Note for PN G339.9+88.4, there is a target within the red circle showing good detections of the [O III] $\lambda\lambda 4959, 5007$ lines but missed in the search. It’s because the intensity ratio of the two lines F_{5007}/F_{4959} is over 4.0.

gions, 1 candidate (SEQ 133) may be associated with the supernova remnant candidate SNR? G107.1+9.0, 1 candidate (SEQ 153) may be a true PN, and 2 candidates (SEQ 136, 149) show nil H α emission. The results indicate that a significant fraction of PN candidates may be (diffuse) H II regions. We also checked the rebinned (about $10''$ per pixel) SDSS g -band images of the candidates. One candidate (SEQ 127) is clearly visible, as shown in Fig. 12, suggesting that it is probably a spherical PN of a radius of about $3.0'$. PG 1204+543, a hot subdwarf O star (Green et al. 1986), is probably its ionizing star.

4 DISCUSSION

4.1 Most highly evolved PNe

The evolved, large PNe play a critical role in studying the transition from PN to white dwarf (e.g. Napiwotzki 1995), the PN-ISM interaction on a range of spatial scales (Tweedy & Kwitter 1994) and calibrating the distances of the diverse population of local PNe (Ciardullo et al. 1999; Frew & Parker 2006; Frew 2008), therefore meriting detailed study. However, such PNe are inherently of low surface brightness and difficult to detect, especially in the Galactic plane where interstellar extinction is large. As mentioned earlier,

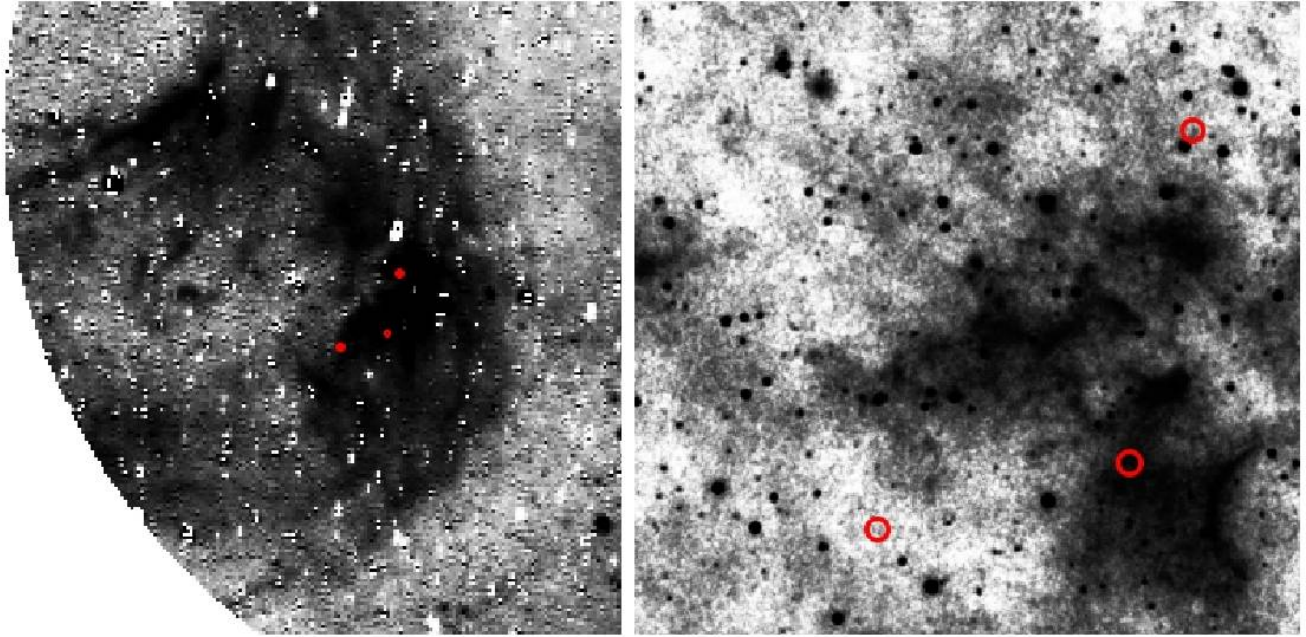


Figure 5. VTSS continuum-corrected $H\alpha$ (left) and WISE $W4$ (right) images of the PN candidate G055.9-3.9. The field of views from left to right are $5.0^\circ \times 5.0^\circ$ and $1.0^\circ \times 1.0^\circ$, respectively. North is up and east is to the left. The circles indicate the positions where the $[\text{O III}] \lambda\lambda 4959, 5007$ lines are detected. This candidate is not a PN but part of an H II region.

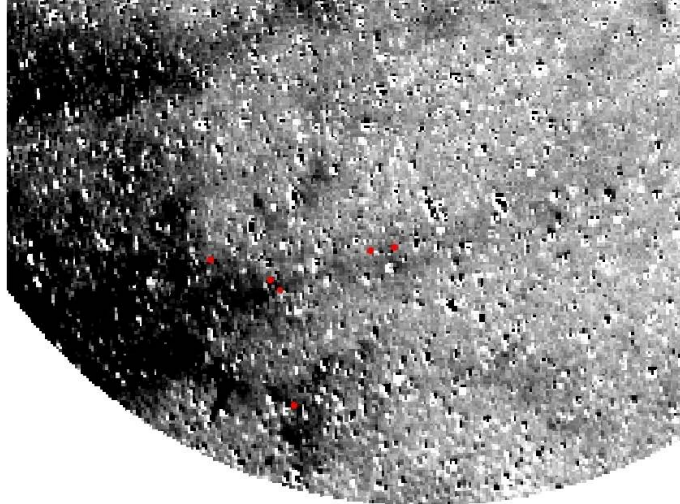


Figure 6. VTSS continuum-corrected $H\alpha$ image of the PN candidate G070.8+10.4. The circles indicate the positions where the $[\text{O III}] \lambda\lambda 4959, 5007$ lines are detected. The field of view is $7.0^\circ \times 5.0^\circ$. North is up and east is to the left. This candidate is probably not a PN but an ionized $H\alpha$ filament associated with an H II region.

the method in this work is mostly sensitive to large and faint PNe, thus very suitable to find most highly evolved PNe.

We have found 7 PN candidates of multiple detections in this work. Based on their spectra and images in $H\alpha$ and other bands, three of them are probably H II regions, one is probably associated with a new supernova remnant, another one is probably a true PN, and the remaining two could be either PNe or supernova remnants. They all exhibit extremely low surface brightness and large sizes, suggesting that they are highly evolved if they are true PNe. Acker

et al. (2012) reported the discovery of a possible PN candidate (Ou4) of the largest angular extent ever found then that extends about $72'$. We have found some PN candidates that are of similar sizes or even larger. Note that the surface brightness of Ou4 is highest in the $[\text{O III}] \lambda 5007$ emission line. It takes a pre-PN 32,600 years to expand to a radius of 0.5 pc at a typical expansion velocity of 30 km/s. Such a PN has an angular extent of 1° at a distance of 57 pc. Thus, we infer that these PN candidates are very old and local ($\lesssim 50$ pc) if their PN nature are confirmed. They

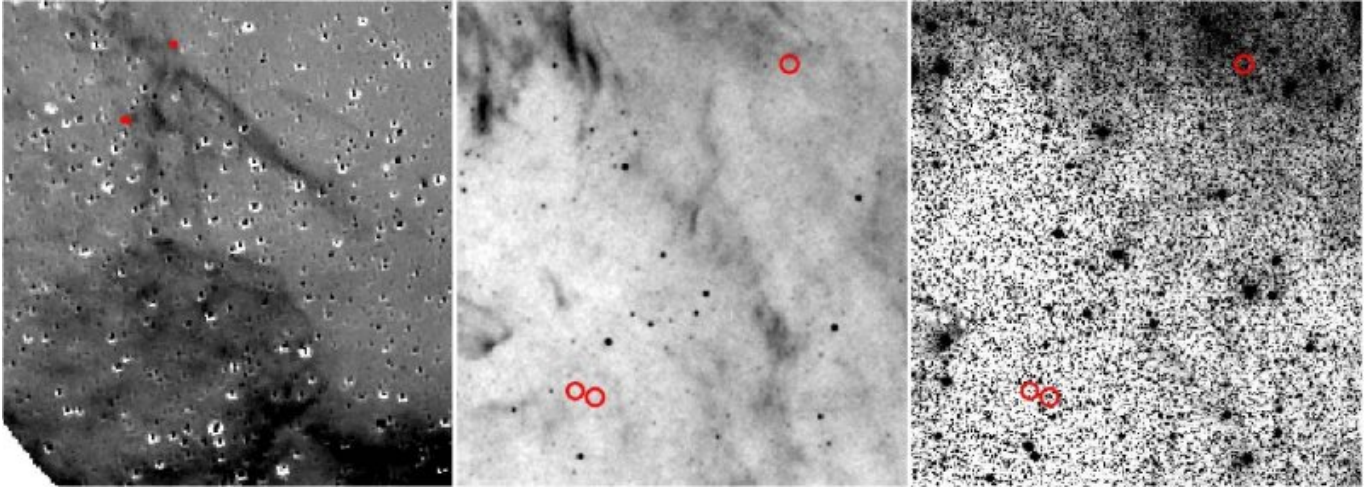


Figure 7. VTSS continuum-corrected $H\alpha$ (left), WISE $W4$ (middle) and DSS-II blue plate (right) images of the PN candidate G108.9+10.7. The field of views from left to right are $3.6^\circ \times 3.6^\circ$, $1.0^\circ \times 1.0^\circ$ and $1.0^\circ \times 1.0^\circ$, respectively. North is up and east is to the left. The circles indicate the positions where the $[O\ III] \lambda\lambda 4959, 5007$ lines are detected. In the bottom-left corner of the VTSS image, there is probably a new supernova remnant (SNR? G107.1+9.0) based on its spherical morphology and filamentary structure. PN? G108.9+10.7 is probably not a PN but associated with this supernova remnant.

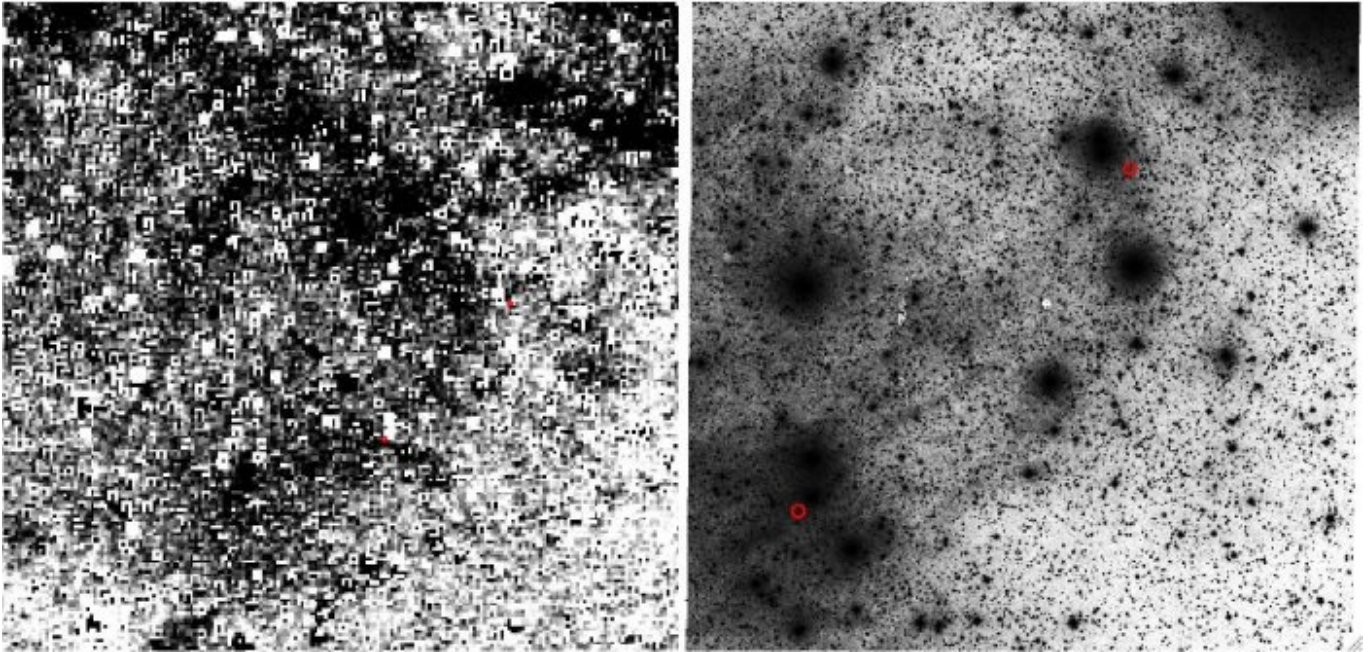


Figure 8. VTSS continuum-corrected $H\alpha$ (left) and DSS-II blue plate (right) images of the PN candidate G117.1–26.3. The field of views from left to right are $5.0^\circ \times 5.0^\circ$ and $2.0^\circ \times 2.0^\circ$, respectively. North is up and east is to the left. The circles indicate the positions where the $[O\ III] \lambda\lambda 4959, 5007$ lines are detected. This candidate is not a PN. The detected $[O\ III]$ emission is from $H\alpha$ filaments of the diffuse ISM.

have radial velocities consistent with disk population (as to be shown in Fig. 14), suggesting that they are descendants of local disk stars.

4.2 A population of faint PNe

Fig. 13 shows histogram distribution of the $[O\ III] \lambda 5007$ line surface brightness S_{5007} measured in this work. The black, red, purple, cyan and blue lines represent the measurements for the total, previously known, haloes of previously known,

multiply-detected and singly-detected PN (candidate) samples, respectively. Note the S_{5007} of the halo PN H 4-1 is 18.14, out of the x-range of this figure. There is not a continuum of S_{5007} from known Halo PNe (e.g. H 4-1) to the strongly clustered faint candidates found in this study. It is probably because that the technique in this work is very biased to large, evolved and faint PNe. The recovery of H 4-1 in this work is lucky, because it is observed as a quasar candidate. Given its small size about $10''$ and the sampling density of SDSS fibers about 100 per sqr.deg. , the proba-

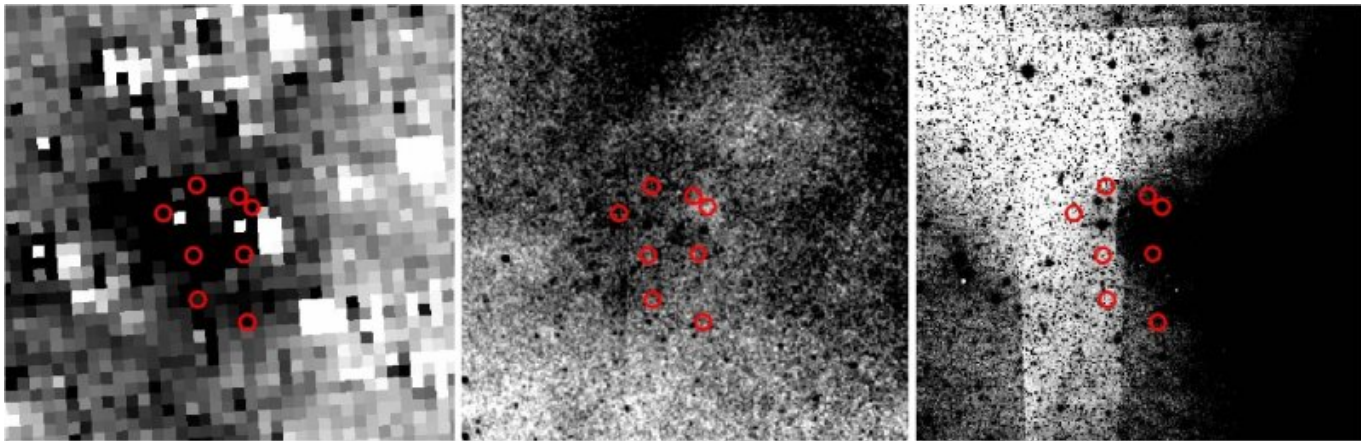


Figure 9. VTSS continuum-corrected $H\alpha$ (left), WISE $W4$ (middle) and DSS-II blue plate (right) images of the PN candidate G126.8–15.5. The field of views are all $1.0^\circ \times 1.0^\circ$. North is up and east is to the left. The circles indicate the positions where the $[O\ III] \lambda\lambda 4959, 5007$ lines are detected. This candidate could be either a PN or a supernova remnant.

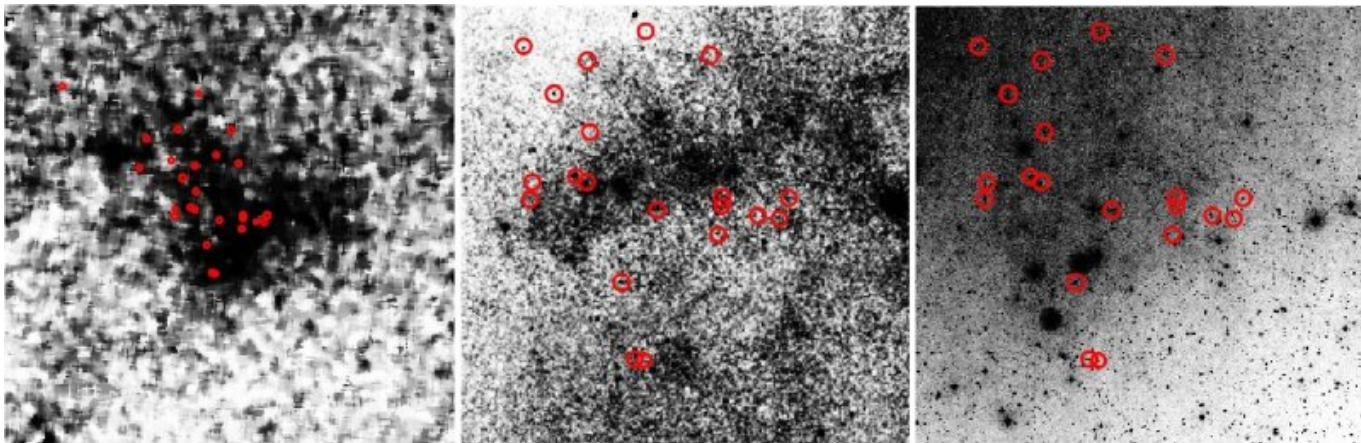


Figure 10. SHASSA continuum-corrected $H\alpha$ (left), WISE $W4$ (middle) and DSS-II blue plate (right) images of the PN candidate G247.7+47.8. The field of views from left to right are $2.7^\circ \times 2.7^\circ$, $1.0^\circ \times 1.0^\circ$ and $1.0^\circ \times 1.0^\circ$, respectively. North is up and east is to the left. The circles indicate the positions where the $[O\ III] \lambda\lambda 4959, 5007$ lines are detected. This candidate is a possible PN.

bility of having such a small PN observed by the SDSS by chance is very tiny, about 0.1 per cent.

Thanks to the extremely high sensitivity of the SDSS spectra in detecting narrow and strong $[O\ III] \lambda\lambda 4959, 5007$ lines from Galactic PNe, we reach PNe of S_{5007} as faint as 29.0 – 30.0 magnitude arcsec^{-2} , much fainter than most previously known PNe. Note that there are a few measurements for the previously known PNe reaching down to $S_{5007} \sim 28.0$ magnitude arcsec^{-2} . But these measurements are for their fainter outer haloes that are firstly discovered in this work.

For an extended source of uniform surface brightness, its surface brightness doesn't depend on its distance if interstellar extinction is not taken into account. Thus, very faint PNe mean that they are very old, large and highly evolved or they are intrinsically fainter than others. Deep imaging and spectroscopic observations are needed to explore the possibilities. All the newly identified PN candidates are very faint, very challenging to be discovered with previously employed techniques (e.g. slitless spectroscopy, narrow-band imaging), and thus may greatly increase the number of "missing" faint PNe.

4.3 Halo PNe

Halo PNe are descendants of stars formed in the early history of the Galaxy. They are important tracers to study the evolution of metal-poor stars and the early physical and chemical conditions of the Galaxy. Halo PNe are mainly characterized by their large height above the Galactic plane, peculiar velocity compared to the Galactic rotation curve of the disk stars and their low metallicity. Currently, very few halo PNe have been identified. There are only 14 PNe from the SECGPN catalog regarded as halo members based on their location and kinematics, including H 4-1 recovered in this work. The SDSS legacy survey concentrates on the Northern Galactic Cap, thus is a very suitable database to search for halo PNe.

To identify possible halo PNe, we plot radial velocities of the SDSS stars and PNe (candidates) as a function of Galactic longitude in Fig. 14. The stars and PNe (candidates) are marked by dots and crosses, respectively. The black dots indicate 30,000 randomly selected metal-rich disk stars of $[\text{Fe}/\text{H}] \geq -0.5$ and the cyan ones indicate 5,000 randomly selected metal-poor halo stars of $[\text{Fe}/\text{H}] \leq -1.5$. The

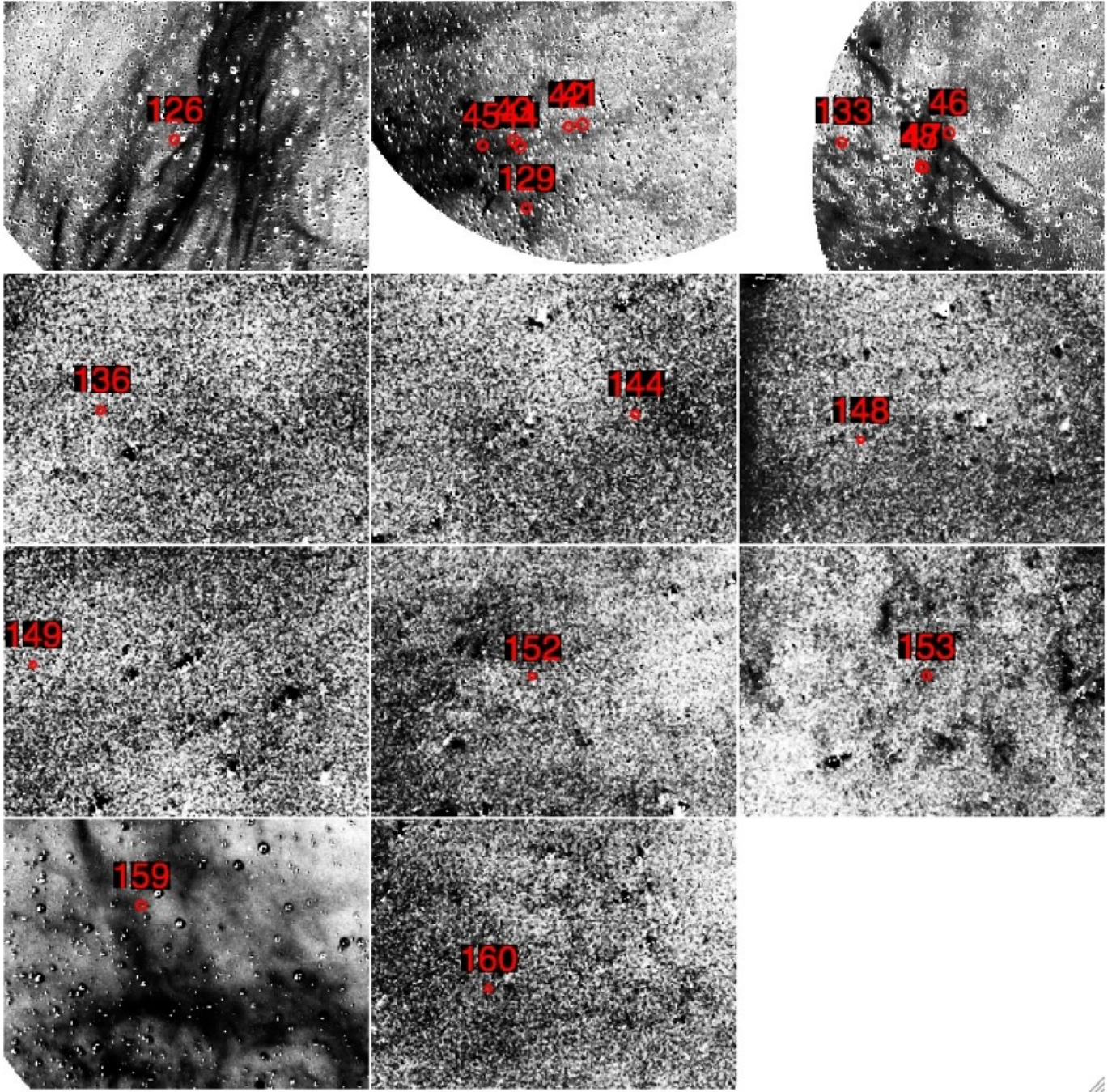


Figure 11. VTSS/SHASS continuum-corrected $H\alpha$ images of 11 PN candidates of single detection. The field of views for the VTSS (SEQ 126, 129, 133, 159) and SHASS (SEQ 136, 144, 148, 149, 152, 153, 160) images are $4.1^\circ \times 3.0^\circ$ and $9.2^\circ \times 6.7^\circ$, respectively. North is up and east is to the left. The circles indicate the positions where the $[O\ III] \lambda\lambda 4959, 5007$ lines are detected and have a radius of $5'$. The SEQs are labeled above the circles.

stars have radial velocity errors smaller than 4.0 km s^{-1} . Here the stellar parameters and their errors are from the SEGUE Stellar Parameter Pipeline (SSPP, Lee et al. 2008a, b; Allende Prieto et al. 2008; Lee et al. 2011; Smolinski et al. 2011). The disk and halo stars are clearly separated in the figure. According to their kinematics, the PNe (candidates) are divided into disk population and halo population, as indicated by red and blue crosses, respectively. In total, 8 halo PNe (candidates) are found and marked in Tab. 1, including

H4-1 and 7 PN candidates. If confirmed, they will greatly increase the number of known halo PNe.

4.4 Total number of Galactic PNe

To estimate the total number of Galactic PNe, a widely used method is based on the identification of a complete sample of PNe within a local volume and then extrapolating that PN density (usually relative to either mass or luminosity)

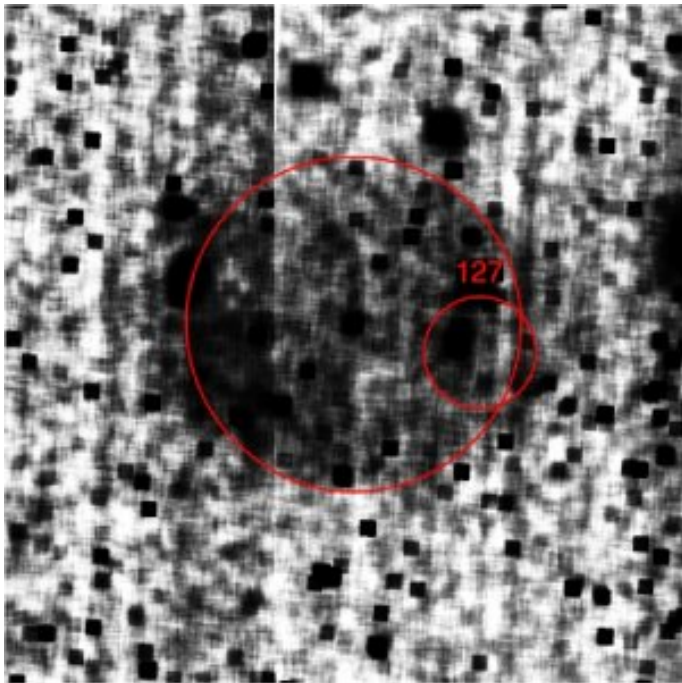


Figure 12. SDSS g -band image of PN? G136.7+61.9 (SEQ 127) after rebinning ($10''$ per pixel). The field of view is $12' \times 12'$. North is up and east is to the left. The small circle indicates the position where the $[\text{O III}] \lambda\lambda 4959, 5007$ lines are detected. The large circle indicates the location and size ($r = 3'$) of the candidate.

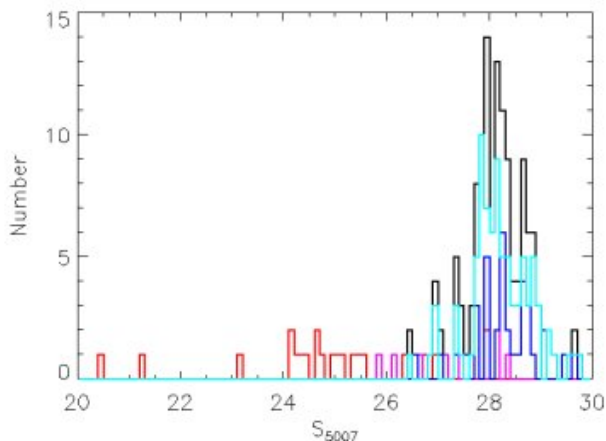


Figure 13. Histogram distribution of the $[\text{O III}] \lambda 5007$ line surface brightness S_{5007} for the total (black), previously known (red), haloes of previously known (purple), multiply-detected (cyan) and singly-detected (blue) PN (candidate) samples, respectively. Note the S_{5007} of the halo PN H 4-1 is 18.14, out of the x-range of this figure.

to the entire Milky Way (e.g. Ishida & Weinberger 1987; Phillips 2002; Frew 2008). Such method requires knowing distances to the local sample. However, accurate PN distances are very difficult to obtain, resulting uncertainties in the estimated total number of Galactic PNe of a factor of 2 – 10. Consequently, this method yields total counts that

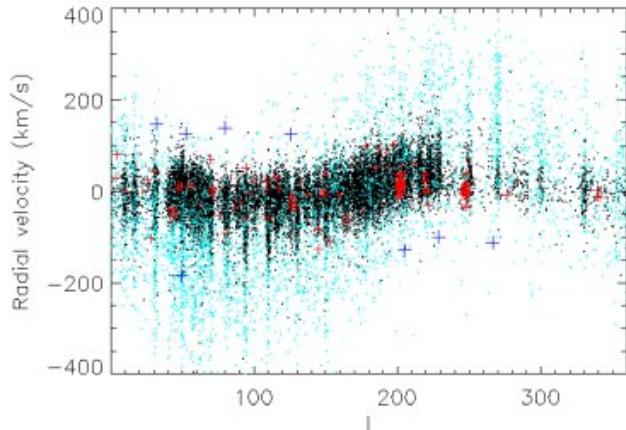


Figure 14. Radial velocities of the SDSS stars and PNe (candidates) as a function of Galactic longitude. The black and cyan dots indicate disk stars of $[\text{Fe}/\text{H}] \geq -0.5$ and halo stars of $[\text{Fe}/\text{H}] \leq -1.5$, respectively. The red and blue crosses indicate disk and halo PNe (candidates), respectively.

have a wide spread in values – from 13,000 (Frew 2008) to 140,000 (Ishida & Weinberger 1987).

With sophisticated modeling of Galactic PN population (e.g. their luminosity and size distributions) and the sampling effects of the SDSS spectroscopic surveys, it is possible to obtain a reliable estimate of the total number of PNe in the Galaxy without knowing distances of PNe. We leave such an exploration to a future paper.

Compared to the SDSS DR7, the SDSS DR9 has increased the number of spectra significantly thanks to the projects SEGUE-II and Baryon Oscillation Spectroscopic Survey (BOSS; Dawson et al. 2013). In addition, the other on-going and up-coming large scale spectral survey projects such as LAMOST (Cui et al. 2012; Zhao et al. 2012; Liu et al. 2013) and HERMES (Freeman 2010) will provide supplementary data-sets for finding PNe (and other types of emission line nebulae) and improving their Galactic census. The search limits can be further increased by using the template subtraction technique, which has been used to detect the diffuse interstellar bands in the SDSS and LAMOST stellar spectra (Yuan & Liu 2012; Yuan et al. 2013). The results of searching for new PNe in the SDSS DR9 and LAMOST datasets will be presented in another work.

5 SUMMARY

We have carried out a systematic search for Galactic PNe by detecting the $[\text{O III}] \lambda\lambda 4959, 5007$ lines in $\sim 1,700,000$ spectra from the SDSS DR7. Thanks to the excellent sensitivity of the SDSS spectroscopic surveys, this is by far the deepest search for PNe ever taken, reaching a surface brightness of the $[\text{O III}] \lambda 5007$ line S_{5007} down to about 29.0 magnitude arcsec^{-2} . A number of interesting results are found:

- we have recovered 13 previously known PNe in the Northern and Southern Galactic Caps, including the halo PN H 4-1. The faint outer haloes of PNe IC 4593, NGC 6210

and NGC 3587 are also recovered, and much larger and fainter than previous findings in the first two cases.

- We have found 7 PN candidates of multiple detections. They all exhibit extremely low surface brightness and large sizes (between $21'$ and $154'$), and are mostly located in the low Galactic latitude region with a kinematics similar to disk stars. Combing their spectra and images in $H\alpha$ and other bands, it's found that three of them are probably H II regions, one is probably associated with a new supernova remnant, another one is a possible PN, and the remaining two could be either PNe or supernova remnants.

- We have found 37 PN candidates of single detection. Seven of them exhibit halo kinematics and may be descendants of halo stars. If confirmed, they will increase the number of known PNe in the Galactic halo significantly.

- All the newly identified PN candidates are very faint, with a surface brightness of the $[O III] \lambda 5007$ line between 27.0 - 30.0 magnitude arcsec^{-2} that is much lower than most previously known PNe. They may greatly increase the number of "missing" faint PNe.

- The results have demonstrated the power of large scale fiber spectroscopy in hunting for ultra-faint PNe and other types of emission line nebulae. Combined with the large spectral databases provided by the SDSS, LAMOST, HERMES and other projects, it will provide a statistically meaningful sample of ultra-faint, large, evolved PNe to improve the census of Galactic PNe.

Acknowledgments We would like to thank the referee for his/her valuable comments, which helped improve the quality of the paper significantly. This work made use of the SDSS and SIMBAD databases. This research made use of Montage, funded by the National Aeronautics and Space Administration's Earth Science Technology Office, Computational Technologies Project, under Cooperative Agreement Number NCC5-626 between NASA and the California Institute of Technology. The code is maintained by the NASA/IPAC Infrared Science Archive. This research made use of the Virginia Tech Spectral-Line Survey (VTSS) and the Southern H-Alpha Sky Survey Atlas (SHASSA), which are supported by the National Science Foundation. This work is supported by the Natural Science Foundation of China (No. 10933001)

REFERENCES

- Abazajian, K. N., Adelman-McCarthy, J. K., Agüeros, M. A., et al. 2009, *ApJS*, 182, 543
- Acker, A., Boffin, H. M. J., Outters, N., et al. 2012, *RMxAA*, 48, 223
- Acker, A., Marcout, J., & Ochsenbein, F. 1996, First Supplement to the SECGPN (Observatoire de Strasbourg)
- Acker, A., Ochsenbein, F., Stenholm, B., et al. 1994, *VizieR Online Data Catalog*, 5084
- Ahn, C. P., Alexandroff, R., Allende Prieto, C., et al. 2012, *ApJS*, 203, 21
- Allende Prieto, C., Sivarani, T., Beers, T. C., et al. 2008, *AJ*, 136, 2070
- Ciardullo, R., Bond, H. E., Sipior, M. S., et al. 1999, *AJ*, 118, 488
- Corradi, R. L. M., Guerrero, M., Manchado, A., & Mampaso, A. 1997, *New Astronomy*, 2, 461
- Cui, X.-Q., Zhao, Y.-H., Chu, Y.-Q., et al. 2012, *Research in Astronomy and Astrophysics*, 12, 1197
- Dawson, K. S., Schlegel, D. J., Ahn, C. P., et al. 2013, *AJ*, 145, 10
- De Marco, O., & Moe, M. 2005, *Planetary Nebulae as Astronomical Tools*, 804, 169
- Dennison, B., Simonetti, J. H., & Topasna, G. A. 1998, *PASA*, 15, 147
- Drew, J. E., Greimel, R., Irwin, M. J., et al. 2005, *MNRAS*, 362, 753
- Freeman, K. C. 2010, *Galaxies and their Masks*, 319
- Frew, D. J. 2008, Ph.D. Thesis
- Frew, D. J., Madsen, G. J., O'Toole, S. J., & Parker, Q. A. 2010, *PASA*, 27, 203
- Frew, D. J., & Parker, Q. A. 2006, *Planetary Nebulae in our Galaxy and Beyond*, 234, 49
- Frew, D. J., & Parker, Q. A. 2010, *PASA*, 27, 129
- Gaustad, J. E., McCullough, P. R., Rosing, W., & Van Buren, D. 2001, *PASP*, 113, 1326
- Gerhard, O. 2006, *Planetary Nebulae in our Galaxy and Beyond*, 234, 25
- Green, R. F., Schmidt, M., & Liebert, J. 1986, *ApJS*, 61, 305
- Haffner, L. M., Reynolds, R. J., Tuft, S. L., et al. 2003, *ApJS*, 149, 405
- Hajian, A. R., Frank, A., Balick, B., & Terzian, Y. 1997, *ApJ*, 477, 226
- Iben, I., Jr. 1995, *Physics Reports*, 250, 2
- Ishida, K., & Weinberger, R. 1987, *A&A*, 178, 227
- Jacoby, G. H. 1989, *ApJ*, 339, 39
- Jacoby, G. H., Kronberger, M., Patchick, D., et al. 2010, *PASA*, 27, 156
- Kniazev, A. Y., Pustilnik, S. A., & Zucker, D. B. 2008, *MNRAS*, 384, 1045
- Kohoutek, L. 2001, *A&A*, 378, 843
- Kwitter, K. B., Downes, R. A., & Chu, Y.-H. 1991, *BAAS*, 23, 914
- Lee, Y. S., Beers, T. C., Allende Prieto, C., et al. 2011, *AJ*, 141, 90
- Lee, Y. S., Beers, T. C., Sivarani, T., et al. 2008a, *AJ*, 136, 2022
- Lee, Y. S., Beers, T. C., Sivarani, T., et al. 2008b, *AJ*, 136, 2050
- Liu, X.-W., et al. 2013, *Setting the scene for Gaia and LAMOST*, in press
- Mathis J. S. & Liu X.-W. 1999, *ApJ*, 521, 212
- Miszalski, B., Parker, Q. A., Acker, A., et al. 2008, *MNRAS*, 384, 525
- Miszalski, B., Acker, A., Ochsenbein, F., & Parker, Q. A. 2012, *IAU Symposium*, 283, 442
- Moe, M., & De Marco, O. 2006, *ApJ*, 650, 916
- Napiwotzki, R. 1995, *White Dwarfs*, 443, 176
- Parker, Q. A., Acker, A., Frew, D. J., et al. 2006, *MNRAS*, 373, 79
- Parker, Q. A., Phillipps, S., Pierce, M. J., et al. 2005, *MNRAS*, 362, 689
- Pottasch, S. R., Bernard-Salas, J., & Roellig, T. L. 2009, *A&A*, 499, 249
- Sabin, L., Parker, Q. A., Contreras, M. E., et al. 2013, *MNRAS*, 431, 279
- Smolinski, J. P., Lee, Y. S., Beers, T. C., et al. 2011, *AJ*, 141, 89
- Stasińska, G., Morisset, C., Tovmassian, G., et al. 2010, *A&A*, 511, A44
- Storey P. J. & Zeippen C. J. 2000, *MNRAS*, 312, 813
- Tweedy, R. W., & Kwitter, K. B. 1994, *AJ*, 108, 188
- Viironen, K., Greimel, R., Corradi, R. L. M., et al. 2009a, *A&A*, 504, 291
- Viironen, K., Mampaso, A., Corradi, R. L. M., et al. 2009b, *A&A*, 502, 113
- Voges, W., Aschenbach, B., Boller, T., et al. 1999, *A&A*, 349, 389

- Wright, E. L., Eisenhardt, P. R. M., Mainzer, A. K., et al. 2010, AJ, 140, 1868
- Yanny, B., Rockosi, C., Newberg, H. J., et al. 2009, AJ, 137, 4377
- York, D. G., Adelman, J., Anderson, J. E., Jr., et al. 2000, AJ, 120, 1579
- Yuan, H.-B., et al. 2013, Setting the scene for Gaia and LAMOST, in press
- Yuan, H.-B. & Liu, X.-W. 2012, MNRAS, 425, 1763
- Zhao, G., Zhao, Y.-H., Chu, Y.-Q., Jing, Y.-P., & Deng, L.-C. 2012, Research in Astronomy and Astrophysics, 12, 723

APPENDIX A: A COLLECTION OF THE SDSS SPECTRA AND IMAGES OF THE TARGETS IN TAB. 1

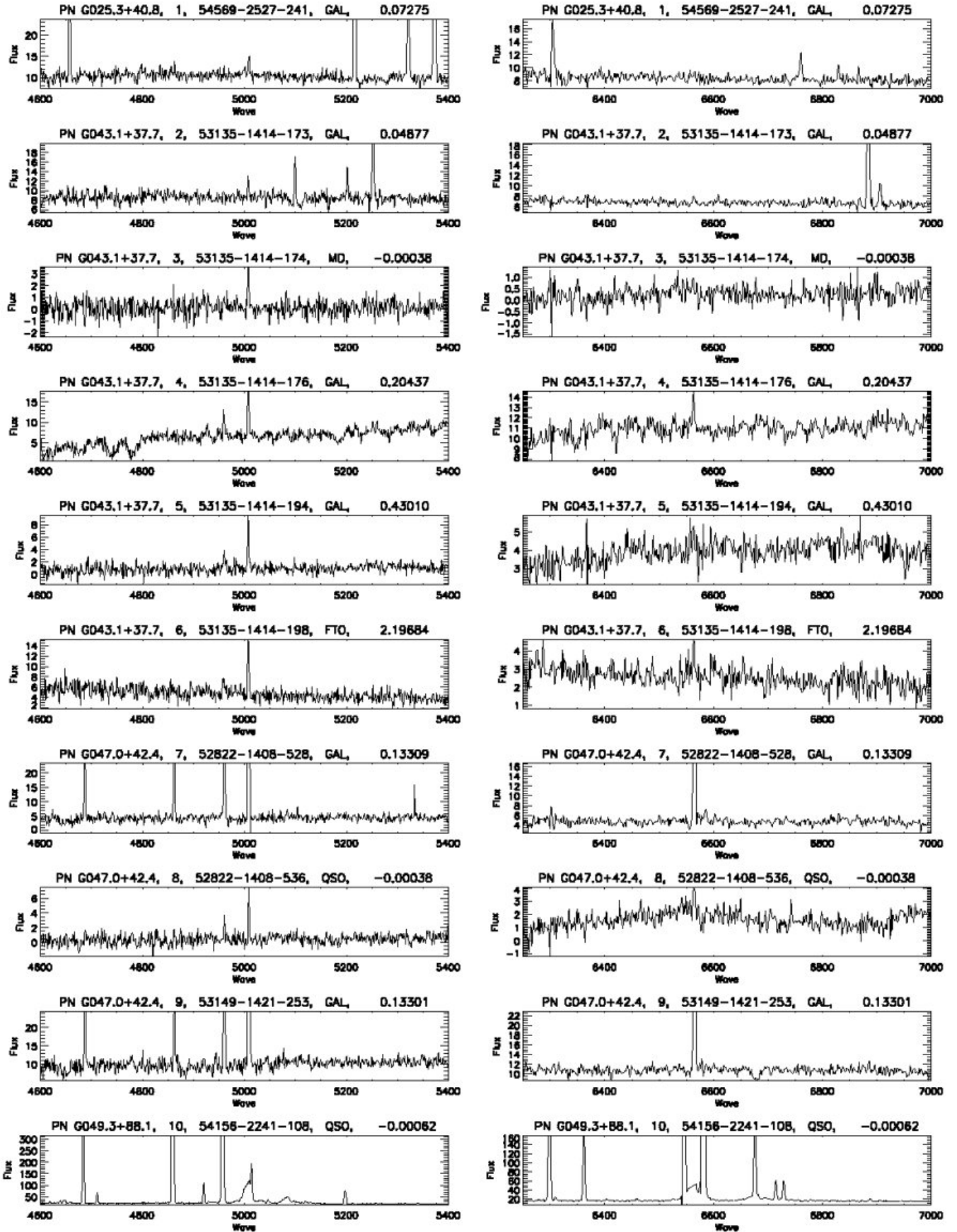


Figure A1. SDSS spectra of the targets in Tab. 1. The PNG identification, SEQ, SDSS spectral ID, initial target type and redshift from Tab. 1 are labeled on the top of each panel. The wavelengths are observed values. The fluxes are in unit of 10^{-17} ergs cm^{-2} s^{-1} \AA^{-1} . The full figure is available online.

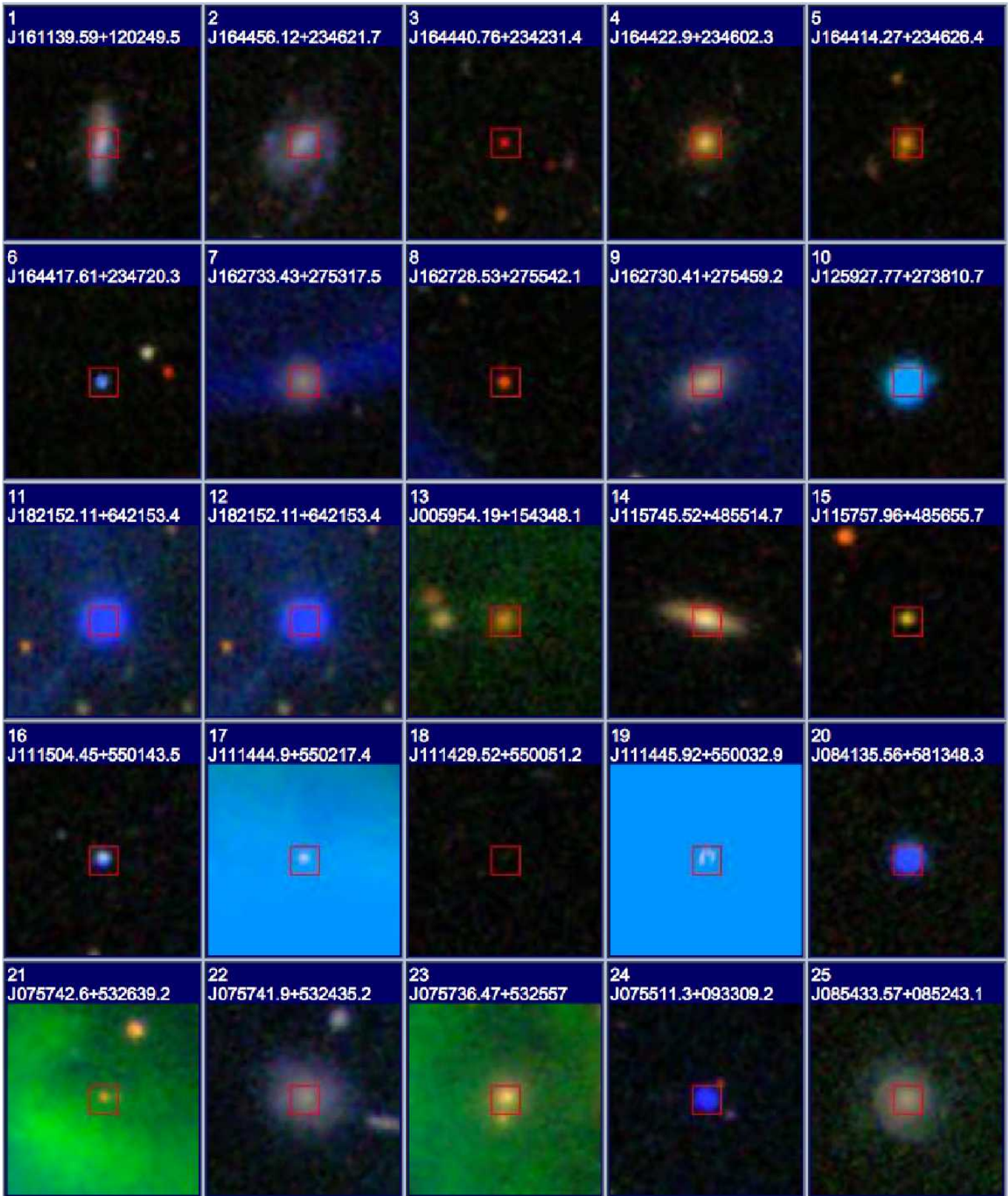


Figure A2. SDSS images of the targets in Tab. 1. The SEQ is labeled on the top of each panel. The full figure is available online.